26

Dynamic Processes in Surfactant-stabilized Emulsions

Krassimir D. Danov, Peter A. Kralchevsky, and Ivan B. Ivanov
University of Sofia, Sofia, Bulgaria

I. INTRODUCTION

The process of emulsification usually takes place under essentially dynamic conditions. It is accompanied with the creation of new drops (new phase boundary) between the two liquids and with frequent collisions between the drops. Their instantaneous size distribution is the result of a competition between two oppositely directed processes: (1) breaking of the drops into smaller ones by the shear strain; and (2) coalescence of the newly formed drops into larger ones upon collision. If *surfactant* is present, it tends to adsorb at the surface of the drops and thus to protect them against coalescence. The rate of surfactant adsorption should be large enough to guarantee obtaining a sufficiently high coverage of the oil-water interface during the short period between two drop collisions. Therefore, an important parameter characterizing a given surfactant as emulsifier is its characteristic *adsorption time* T_1; the latter can vary by many orders of magnitude depending on the type of surfactant, its concentration, and the presence or absence of added nonamphiphilic electrolyte (salt) in the aqueous phase. In Sec. II.B we demonstrate how to quantify T_1 for both ionic and nonionic surfactants.

The adsorbed surfactant molecules counteract the drop coalescence in two ways (1, 2). The presence of surfactant gives rise to repulsive surface forces (of either electrostatic, steric, or oscillatory structural origin) between the drops, thus providing a *thermodynamic* stabilization of the emulsion; see also Refs 3 and 4. Moreover, the adsorbed surfactant reduces (or completely removes) the tangential mobility of the drop surfaces and in this way markedly decelerates the interdroplet collisions; this is known as *kinetic* stabilization (1). The latter is related to the Marangoni effect, i.e., to the appearance of gradients of adsorption and interfacial tension along the surfaces of two colliding droplets (see Fig. 1):

$$\nabla_s \sigma = -\frac{E_G}{\Gamma_1} \nabla_s \Gamma_1 \qquad (1)$$

where V_s is the surface gradient operator, Γ is the surface tension, T_1 is the surfactant adsorption, and E_G the Gibbs (surface) elasticity; expressions for estimating E_G can be found in Sec. II.A.

In the case of low interfacial coverage with surfactant, the collision of two emulsion drops (step A→B in Fig. 2) usually terminates with their coalescence (step B→C in Fig. 2). The merging of the two drops occurs when a small critical distance between their surfaces, h_c is reached. Sometimes, depending on the specifie conditions (larger drop size, attractive surface forces, smaller surface tension, etc., —- see, e.g., Ref. 2), the approach of the two drops could be accompanied with a deformation in the zone of their contact (step B→D in Fig. 2); in this way a *liquid film* of almost uniform thickness *h* is formed in the contact zone. This film could also have a critical thickness h_c of rupture; in fact, the film rupture is equivalent to drop coalescence (see step D→C in Fig. 2). The mechanisms of coalescence

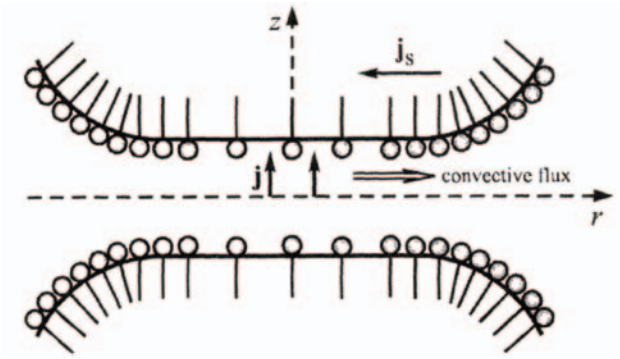

Figure 1 Schematic presentation of the zone of contact between two approaching emulsion drops. The convective outflow of liquid from the gap between the drops drags the surfactant molecules along the two film surfaces: j and j_S denote the bulk- and surface-diffusion fluxes of surfactant.

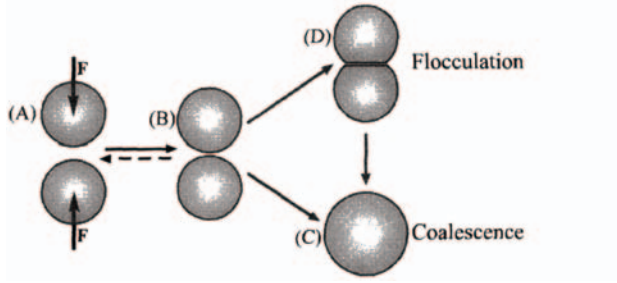

Figure 2 Possible consequences from a collision between two emulsion drops. Step A → B: the two drops approach each other under the action of a driving force F; the viscous friction, accompanying the expulsion of liquid from the gap between the two drops, decelerates their approach. Step B → C: after reaching a given *critical distance* between the two drop surfaces coalescence takes place. Step B → D: after reaching a given threshold distance, h_{inv}, between the two drop surfaces, called the *inversion thickness*, the spherical drops deform and a film is formed in the zone of their contact. Step D → C: the film, intervening between the two drops, thins and eventually breaks after reaching a certain *critical thickness*, then the two drops coalesce.

and the theoretical evaluation of h_c are considered in Sec. III.

The driving force of the drop—-drop collisions (F in Fig. 2) can be the Brownian stochastic force, the buoyancy force, or some attractive surface force (say, the van der Waals interaction); in stirred vessels an important role is played by the hydrodynamic (including turbulent) forces. The mutual approach of two emulsion drops (step A→B in Fig. 2) is decelerated by the *viscous friction* due to the expulsion of the liquid from the gap between the drops. If a doublet of two drops (Fig. 2D) is sufficiently stable, it can grow by attachment of additional drops; thus, aggregates of drops (floes) are produced.

If the stirring of an emulsion is ceased, there is no longer generation of new droplets, but the opposite processes of drop flocculation and/or coalescence continue. After some period of time this will lead to the appearance of sufficiently large floes and/or drops, for which the gravitational force is stronger than the Brownian force; this will lead to a directional motion of the drops/floes upwards (creaming) or downwards (sedimentation), depending on whether the buoyancy force or the drop weight prevails.

As an illustrative example, Fig. 3 shows the occurrence of the creaming in an oil-in-water emulsion stabilized by the protein βS-lactoglobulin —- data from Ref. 5. The rise of the boundary between the lower transparent aqueous phase (serum) and the upper turbid emulsion phase is recorded as a function of time; in particular, the ratio of the volume of the serum to the total volume (turbid plus transparent phase) is plotted versus time. Two types of emulsions are used in these experiments: "coarse" and "fine" emulsion of average drop size 5 and 0.35 μrn, respectively. In Fig. 3 one sees that, in *the fine* emulsion, creaming is not observed (the volume of the separated serum is zero). In contrast, there is creaming in the *coarse* emulsion, which starts some time after the initial moment (the ceasing of agitation); this period is necessary for "incubation" of suffi-

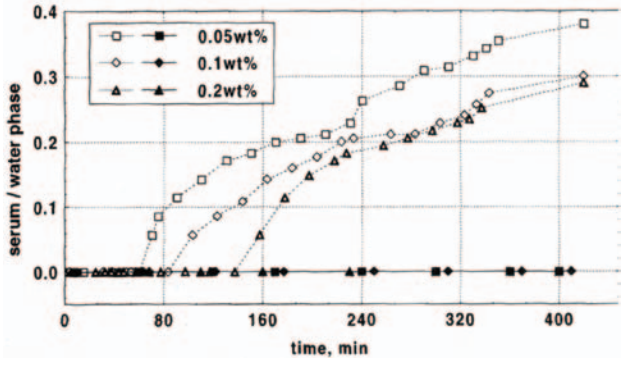

Figure 3 Experimental data for creaming in xylene-in-water emulsions. The volume of the transparent "serum" left below the creaming emulsion, scaled with the total volume of the liquid mixture, is plotted against the time elapsed after ceasing the agitation. The emulsion is stabilized with β-lactoglo-bulin, whose concentrations, corresponding to the separate curves, are shown in the figure. The empty and full symbols denote, respectively, "coarse" emulsion (mean drop size 5μm) and "fine" emulsion (mean drop size 0.35 μm).

ciently large floes, which are able to emerge under the action of the buoyancy force. The stabilizing effect of SbT-lactoglobulin is manifested as an increase in the "incubation period" with the rise of protein concentration.

The theoretical description of the mutual approach and coalescence of two emulsion drops is the subject of Sec. IV; the Bancroft rule on emulsiflcation is interpreted and generalized in Sec. V; and the kinetics of flocculation is considered in Sec. VI, where the size of the aggregates needed for the creaming to start is estimated.

II. DYNAMICS OF SURFACTANT ADSORPTION MONOLAYERS

A. Gibbs (Surface) Elasticity

1. Nonionic Surfactant Solutions

Let us consider the boundary between an aqueous solution of a nonionic surfactant and the oil phase. We choose the dividing surface to be the equimolecular dividing surface with respect to water. The Gibbs adsorption equation then takes the form (6, 7):

$$d\sigma = kT\,\Gamma_1\, d\ln c_1 \tag{2}$$

where the subscript "1" denotes the nonionic surfactant, C_1 and T_1 are its bulk concentration and adsorption, k is the Boltzmann constant, and T is the temperature. The surfactant adsorption isotherms, expressing the connection between T_1 and c_1, are usually obtained by means of some molecular model of the adsorption. The most popular is the Langmuir (8) adsorption isotherm;

$$\frac{\Gamma_1}{\Gamma_\infty} = \frac{Kc_1}{1+Kc_1} \tag{3}$$

which stems from a lattice model of localized adsorption of *noninteracting* molecules (9). In Eq. (3) Γ_∞ is the maximum possible value of the adsorption ($\Gamma_1 \to \Gamma_\infty$ for $c_1 \to \infty$). On the other hand, for $c_1 \to 0$ one has $\Gamma_1 \approx Kc_1$; the adsorption parameter K characterizes the surface activity of the surfactant: the greater K the higher the surface activity.

Table 1 lists the six most popular surfactant adsorption isotherms, i.e., those of Henry, Freundlich, Langmuir, Volmer (10), Frumkin (11), and van der Waals (9). For $c_1 \to 0$ all other isotherms (except that of Freundlich) reduce to the Henry isotherm. The physical difference between the Langmuir and Volmer isotherms is that the former corresponds to a physical model of *localized* adsorption, whereas the latter corresponds to *nonlocalized* adsorption. The Frumkin and van der Waals isotherms generalize, respectively, the Langmuir and Volmer isotherms for the case when there is interaction between the adsorbed molecules; β is a parameter which accounts for the interaction. In the case of the van der Waals interaction, β can be expressed in the form (12, 13):

Table 1 The Most Popular Surfactant Adsorption Isotherms and the Respective Surface Tension Isotherms; c_{1s} is the Subsurface Concentration of Surfactant Molecules

	Sufactant adsorption isotherms (for nonionic surfactants: $Kc_{1s} \equiv c_1$)
Henry	$Kc_{1s} = \frac{\Gamma_1}{\Gamma_\infty}$
Freundlich	$Kc_{1s} = \left(\frac{\Gamma_1}{\Gamma_F}\right)^{1/m}$
Langmuir	$Kc_{1s} = \frac{\Gamma_1}{\Gamma_\infty - \Gamma_1}$
Volmer	$Kc_{1s} = \frac{\Gamma_1}{\Gamma_\infty - \Gamma_1}\exp\left(\frac{\Gamma_1}{\Gamma_\infty - \Gamma_1}\right)$
Frumkin	$Kc_{1s} = \frac{\Gamma_1}{\Gamma_\infty - \Gamma_1}\exp\left(-\frac{2\beta\Gamma_1}{kT}\right)$
Van der Waals	$Kc_{1s} = \frac{\Gamma_1}{\Gamma_\infty - \Gamma_1}\exp\left(\frac{\Gamma_1}{\Gamma_\infty - \Gamma_1} - \frac{2\beta\Gamma_1}{kT}\right)$
	Surface tension isotherm $\sigma = \sigma_0 - kTJ + \sigma_d$ (for nonionic surfactants: $\sigma_d \equiv 0$)
Henry	$J = \Gamma_1$
Freundlich	$J = \frac{\Gamma_1}{m}$
Langmuir	$J = -\Gamma_\infty \ln\left(1 - \frac{\Gamma_1}{\Gamma_\infty}\right)$
Volmer	$J = \frac{\Gamma_\infty \Gamma_1}{\Gamma_\infty - \Gamma_1}$
Frumkin	$J = -\Gamma_\infty \ln\left[\left(1 - \frac{\Gamma_1}{\Gamma_\infty}\right) - \frac{\beta\Gamma_1^2}{kT}\right]$
van der Waals	$J = \frac{\Gamma_\infty \Gamma_1}{\Gamma_\infty - \Gamma_1} - \frac{\beta\Gamma_1^2}{kT}$

$$\beta = -\pi kT \int_{r_0}^{\infty}\left[1 - \exp\left(-\frac{u(r)}{kT}\right)\right]dr \approx -\pi \int_{r_0}^{\infty} u(r)\, r\, dr \tag{4}$$

where u(r) is the interaction energy between two adsorbed molecules, and r_0 is the distance between the centers of the molecules at close contact. The comparison between theory

and experiment shows that the interaction parameter β is important for air—-water interfaces, whereas for oil—-water interfaces one can set β = 0 (14, 15). The latter fact, and the finding that β > 0 for air-water interfaces, leads to the conclusion that β takes into account the van der Waals attraction between the hydrocarbon tails of the adsorbed surfactant molecules across air (such attraction is missing when the hydrophobic phase is oil). Note, however, that even for an oil-water interface one could have β < 0 if some nonelectrostatic repulsion between the adsorbed surfactant molecules takes place, say steric repulsion between some chain branches of amphiphilic molecules with a more complicated structure.

Concerning the parameter K in Table 1, this is related to the standard free energy of adsorption, $\Delta f = \mu - \mu$, which is the energy gain for bringing a molecule from the bulk of the water phase to a diluted adsorption layer (3, 16):

$$K = \frac{\delta_1}{\Gamma_\infty} \exp\left[\frac{\mu_1^{(0)} - \mu_{1s}^{(0)}}{kT}\right] \tag{5}$$

Here, δ_1 is a parameter, characterizing the thickness of the adsorption layer, which can be set (approximately) equal to the length of the amphiphilic molecule. Let us consider the integral:

$$J \equiv \int_0^{c_1} \Gamma_1 \frac{dc_1}{c_1} = \int_0^{\Gamma_1} \Gamma_1 \frac{d\ln c_1}{d\Gamma_1} d\Gamma_1 \tag{6}$$

The derivative $d \ln c_1/dT_1$ can be calculated for each adsorption isotherm in Table 1 and then the integration in Eq. (6) can be carried out analytically (17). The expressions for J thus obtained are also listed in Table 1. The integration of the Gibbs adsorption isotherm, Eq. (2), along with Eq. (6), yields (17):

$$\sigma = \sigma_0 - kTJ \tag{7}$$

which in view of the expressions for J in Table 1 presents the surfactant adsorption isotherm, or the two-dimensional (surface) equation of state.

As mentioned in the Sec. I, an important thermo-dynamic parameter of a surfactant adsorption monolayer is its Gibbs (surface) elasticity. The physical concept of surface elasticity is the most transparent for monolayers of *insoluble* surfactants, for which it was initially introduced by Gibbs (18, 19). The increments $\Delta\sigma$ and $\Delta\Gamma_1$ in the definition of Gibbs elasticity:

$$E_G = -\Gamma_1 \lim_{\Delta\Gamma_1 \to 0}\left(\frac{\Delta\sigma}{\Delta\Gamma_1}\right) = -\Gamma_1\left(\frac{\partial\sigma}{\partial\Gamma_1}\right)_T \tag{8}$$

correspond to variations in surface tension and adsorption during a real process of interfacial dilatation. Expressions for E_G, corresponding to various adsorption isotherms, are shown in Table 2. As an example, let us consider the expression for E_g, corresponding to the Langmuir isotherm; combining the results from Tables 1 and 2 one obtains:

$$E_G = \Gamma_\infty kT\, Kc_1 \qquad \text{(for Langmuir isotherm)} \tag{9}$$

One sees that for Langmuirian adsorption the Gibbs elasticity grows linearly with the surfactant concentration c_1. Since the concentration of the monomeric surfactant cannot exceed the critical micellization concentration, $C_1 \le C_{CMC}$, then from Eq. (9) one obtains:

$$E_G \le (E_G)_{\max} = \Gamma_\infty kTKc_{CMC} \qquad \text{(for Langmuir isotherm)} \tag{10}$$

Hence, one could expect higher elasticity E_G for surfactants with higher C_{CMC}; this conclusion is consistent with the experimental results (20).

The Gibbs elasticity characterizes the lateral fluidity of the surfactant adsorption monolayer. For high values of the Gibbs elasticity the adsorption monolayer at a fluid interface behaves as tangentially immobile. Then, if two oil drops approach each other, the hydro-dynamic flow pattern, and the hydrodynamic interaction as well, is the same as if the drops were solid particles, with the only difference that under some conditions they could deform in the zone of contact. For lower values of the Gibbs elasticity the

Table 2 Expressions for the Gibbs Elasticity of Adsorption Monolayers (Valid for Both Nonionic and Ionic Surfactants), Which Correspond to the Various Types of Isotherms in Table 1

Type of surface tension isotherm	Gibbs elasticity E_G
Henry	$E_G = kT\,\Gamma_1$
Freundlich	$E_G = kT\frac{\Gamma_1}{m}$
Langmuir	$E_G = kT\,\Gamma_1\frac{\Gamma_\infty}{\Gamma_\infty - \Gamma_1}$
Volmer	$E_G = kT\,\Gamma_1\frac{\Gamma_\infty^2}{(\Gamma_\infty - \Gamma_1)^2}$
Frumkin	$E_G = kT\,\Gamma_1\left[\frac{\Gamma_\infty}{\Gamma_\infty - \Gamma_1} - \frac{2\beta\Gamma_1}{kT}\right]$
van der Waals	$E_G = kT\,\Gamma_1\left[\frac{\Gamma_\infty^2}{(\Gamma_\infty - \Gamma_1)^2} - \frac{2\beta\Gamma_1}{kT}\right]$

Marangoni effect appears, see Eq. (1), which can considerably affect the approach of the two drops. These aspects of the hydrodynamic interactions between emulsion drops are considered in Sec. IV.

In the case of a soluble nonionic surfactant the detected increase in a in a real process of interfacial dilatation can be a pure manifestation of surface elasticity only if the period of dilatation,Δt, is much shorter than the characteristic relaxation time of surface tension τ_σ, $\Delta t \ll \tau_\sigma$ (21). Otherwise, the adsorption and the surface tension would be affected by the diffusion supply of surfactant molecules from the bulk of solution toward the expanding interface. The diffusion transport tends to reduce the increase in surface tension upon dilatation, thus apparently rendering the interface less elastic and more fluid. The initial condition for the problem of adsorption kinetics involves an "instantaneous" ($\Delta t \ll \tau_\sigma$) dilatation of the interface. This "instantaneous" dilatation decreases the adsorptions Γ_i; and the subsurface concentrations c_{is} of the species (the subsurface is presumed to be always in equilibrium with the surface), but the bulk concentrations $c_{i\infty}$ remain unaffected (22—24). This initially created difference between c_{is} and $c_{i\infty}$ further triggers the diffusion process. Now, let us inspect closer how this approach is to be extended to the case of ionic surfactants.

2. Ionic Surfactant Solutions

The thermodynamics of adsorption of *ionic* surfactants is more complicated due to the presence of long-range electrostatic interactions in the system. Let us consider a boundary between two immiscible fluid phases (say, water and oil), which bears some electric charge owing to the adsorption of charged amphiphilic molecules (ionic surfactant). The charged surface repels the *colons*, i.e., ions having a charge of the same sign, but it attracts the *counterions*, which bear a charge of the opposite sign (Fig. 4). Thus, an electric double layer (EDL) appears, that is, a nonuniform distribution of the ionic species in the vicinity of the charged interface (25). The conventional model of the EDL stems from the works of Gouy (26), Chapman (27), and Stern (28). According to this model the EDL consists of two parts: (1) *adsorption layer*; and (2) *diffuse layer* (see Fig. 4). The adsorption layer includes surfactant molecules, which are immobilized (adsorbed) at the phase boundary, as well as bound counterions, which form the Stern layer. The diffuse layer consists of free ions in the aqueous phase, which are involved in Brownian motion and are influenced by the electric field of the charged interface. The boundary, separating the adsorption from the diffuse layer, called the *Gouy plane*, can be used as a Gibbs dividing surface between the two neighboring phases (15). The electric potential varies across the EDL: $\psi = \psi(x)$. The boundary values of $\psi(x)$ are $\psi(x = 0) = \psi_s$ at the Gouy plane (at the interface) and $\psi(x \to \infty) = 0$ in the bulk of the solution. At equilibrium, the subsurface concentrations of the ionic species, c_{is}, are related to the respective bulk concentrations, $c_{i\infty}$, by means of the Boltzmann distribution (25):

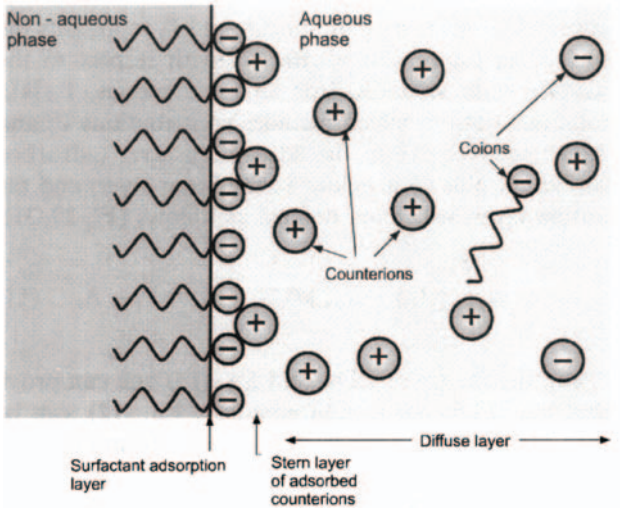

Figure 4 EDL formed in the vicinity of an adsorption monolayer of ionic surfactant. The diffuse layer contains free ions involved in Brownian motion, while the Stern layer consists of adsorbed (immobilized) counterions. Near the charged surface there is an accumulation of counterions and a depletion of coions.

$$c_{is} \equiv c_i(x = 0) = c_{i\infty} \exp\left[-\frac{z_i e \psi_s}{kT}\right] \qquad (11)$$

where $i = 1, 2, 3, \ldots, N$. Here, e is the electronic charge, and z_i, is the valency of the z'th ion. The Gibbs adsorption equation can be presented in the form (15, 17, 29—31):

$$d\sigma = -kT \sum_{i=1}^{N} \tilde{\Gamma}_i d \ln c_{i\infty} \qquad (T = \text{constant}) \quad (12)$$

Equations (11) and (12) are rigorous in terms of activities of the ionic species, rather than in terms of concentrations. For simplicity, here we set the activities equal to the concentrations, which is a good approximation for ionic strengths below 0.1 M; see Refs 14, 15 and 17 for details. In Eq. (12), Γ_i,denotes the adsorption of the z'th compo-

nent, and Γ_i, represents the surface excess of component "i" with respect to the *uniform* bulk solution. For an ionic species, Γ_i is a total adsorption, which includes contributions Γ_i and Λ_i, respectively, from the adsorption layer (adsorbed surfactant plus counterions in the Stern layer) and the diffuse layer, which are denned as follows (17, 29—31):

$$\Lambda_i \equiv \int_0^\infty [c_i(x) - c_{i\infty}]dx, \qquad \Gamma_i \equiv \tilde{\Gamma}_i - \Lambda_i \tag{13}$$

Using the theory of EDL and Eq. (13) one can prove that the Gibbs adsorption equation, Eq. (12), can be represented in the following equivalent form (17):

$$d\sigma_a = -kT\sum_{i=1}^{N}\Gamma_i d\ln c_{is} \qquad (T = \text{constant}) \tag{14}$$

where $\sigma_a = \sigma - \sigma_d = \sigma_0 - kTJ$ is the contribution of the *adsorption* layer to the surface tension [J is the same as in Eq. (6) and Table 1], and σ_b is the contribution of the *diffuse* layer (17, 29):

$$\sigma_d = -\frac{\varepsilon}{4\pi}\int_0^\infty \left(\frac{\partial\psi}{\partial x}\right)^2 dx \tag{15}$$

where ε is the dielectric permittivity of the aqueous phase. The integrand in Eq. (15) represents the aniso-tropy of the Maxwell electric stress tensor, which contributes to the interfacial tension in accordance with the known Bakker formula (32—34). The comparison between Eqs (12) and (14) shows that the Gibbs adsorption equation can be expressed either in terms of σ, Γ_i,, and $c_{i\infty}$, or in terms of σ_a, $_i$, and c_{is}. The total surface tension is

$$\sigma = \sigma_a + \sigma_d \tag{16}$$

Note that σ_b represents a nonlocal, integral contribution of the whole diffuse EDL, whereas σ_a is related to the two-dimensional state of the adsorbed surfactant ions and bound counterions (Fig. 4).

Let us consider a solution of ionic surfactant, which is a symmetric $z{:}z$ electrolyte, in the presence of additional non-amphiphilic $z{:}z$ electrolyte (salt); here, $z \equiv z_1 = -z_2 = z_3$. We assume that the counterions due to the surfactant and salt are identical. For example, this can be a solution of sodium dodecyl sulfate (SDS) in the presence of NaCl. We denote by $c_{1\infty}$, $c_{2\,\infty}$, and $c_{3\,\infty}$ the bulk concentrations of the surface active ions (1), counterions (2), and coions (3), respectively. For the special system of SDS with NaCl $c_{1\,\infty}$, $c_{2\,\infty}$, and $c_{3\,\infty}$ are the bulk concentration of the DS^-, Na^+, and Cl^- ions, respectively. The requirement for the bulk solution to be electroneutral implies that $c_{2\,\infty} = c_{1\,\infty} + c_{3\,\infty}$. The binding of *coions* due to the non-amphiphilic salt is expected to be equal to zero, $\Gamma_3 = 0$, because they are repelled by the similarly charged interface (17). However, $A_3 \neq 0$; hence, $\Gamma_3 = A_3 \neq 0$. The difference between the adsorptions of surfactant ions and counterions determines the surface charge density, $\rho_s = ez(\Gamma_1 - \Gamma_2)$. For the considered system, Eq. (11) can be presented in the form:

$$c_{is} = c_{i\infty}\exp[(-1)^i\phi_s], \qquad \phi_s \equiv \frac{ze\psi_s}{kT} \tag{17}$$

(i = 1, 2, 3). Note that the dimensionless surface electric potential $ø_s$ thus defined is always positive, irrespective of whether the surfactant is cationic or anionic.

Let us proceed with the definition of Gibbs elasticity for an adsorption monolayer from *ionic* surfactant. The main question is whether or not the electric field in the EDL should be affected by the "instantaneous" dilatation of the interface, —- $\Delta\Gamma_1$; which is involved in the definition of E_G - see Eq. (8). This problem has been examined in Ref. 35 and it has been established that a variation of the electric field during the initial instantaneous dilatation leads to results that are unacceptable from a theoretical viewpoint. The latter conclusion is related to the following facts: (1) the speed of propagation of the electric signals is much greater than the characteristic rate of diffusion; and (2) even a small initial variation in the surface charge density ρ_s immediately gives rise to an electric potential, which is linearly increasing with the distance from the interface (potential of a planar wall). Consequently, a small initial perturbation of the interface would immediately affect the ions in the *whole* solution; of course, such an initial condition is physically unacceptable. In reality, a linearly growing electric field could not appear in an ionic solution, because a variation of the surface-charge density would be immediately suppressed by exchange of counterions, which are abundant in the subsurface layer of the solution. The theoretical equations suggest the same (35): to have a mathematically meaningful initial condition of *small* perturbation for the diffusion problem, the initial dilatation must be carried out at constant surface-charge density ρ_s; for details see the Appendix in Ref. 35. Thus, the following conclusion has been reached: the initial sudden inter-facial dilatation, which is related to the definition of Gibbs elasticity of a soluble ionic surfactant, must be carried out at ρ_s = constant. From Eq. (16) one obtains (36):

$$(d\sigma)_{\rho_s} = (d\sigma_a)_{\rho_s} + (d\sigma_d)_{\rho_s} \tag{18}$$

An interfacial dilatation at constant ρ_S does not alter the diffuse part of the EDL, and consequently, $(d\sigma_d)_\rho$ ρ 0, see Eq. (15). Since (17),

$$\sigma_a = \sigma_0 - kTJ \tag{19}$$

the expressions for J in Table 1 show that σ_a depends only on Γ_1 at constant temperature. The definition of Gibbs elasticity of nonionic adsorption layers can then be extended to ionic adsorption layers in the following way (36):

$$E_G \equiv -\Gamma_1 \left[\frac{\partial\sigma}{\partial\Gamma_1}\right]_{T,\rho_s} = -\Gamma_1 \left[\frac{\partial\sigma_a}{\partial\Gamma_1}\right]_T \tag{20}$$
(ionic surfactant)

The definition of Gibbs elasticity given by Eq. (19) corresponds to an "instantaneous" ($\Delta t \ll \tau_\sigma$) dilatation of the *adsorption* layer (that contributes to σ_a) without affecting the *diffuse* layer and σ_d. The dependence of σ on Γ_1 for nonionic surfactants is the same as the dependence of σ_a on Γ_1 for ionic surfactants, cf. Eqs (7) and (19). Equations (8) and (20) then show that the expressions for E_G in Table 2 are valid for *both* nonionic and ionic surfactants. The effect of the surface electric potential on the Gibbs elasticity E_G of an ionic adsorption monolayer is implicit, through the equilibrium surfactant adsorption Γ_1; which depends on the electric properties of the interface. To illustrate this let us consider the case of Langmuir adsorption isotherm for an *ionic* surfactant (17):

$$Kc_{1s} = \frac{\Gamma_1}{\Gamma_\infty - \Gamma_1}, \qquad K \equiv K_1 + K_2 c_{2s} \tag{21}$$

where K_1 and K_2 are constants. Note that the above linear dependence of the adsorption parameter K on the subsurface concentration of counterions, c_{2S}, can be deduced from the equilibrium exchange reactions, which describe the adsorption of surfactant ions and counterions (see Ref. 37). Combining the respective expression from Table 2 with Eq. (21) we obtain $E_G = \Gamma_\infty kTKc_{1S}$. Further, having in mind that $K = K_1 + K_2\, c_{2S}$, we substitute Eq. (17) to derive

$$E_G = \Gamma_\infty kTc_{1\infty}[K_1 \exp(-\phi_s) + K_2\, c_{2\infty}] \tag{22}$$
(for Langmuir isotherm)

Equation (22) reveals the effect of salt on E_G: when the salt concentration increases, $c_{2\infty}$ also increases, whereas the (dimensionless) surface potential $ø_s$ decreases (see Fig. 5, from Ref. 17); then, Eq. (22) predicts an increase in E_G with the rise in salt concentration.

A numerical illustration of the latter prediction is given in Fig. 4. The Gibbs elasticity is calculated with the help of Eq. (22), i.e., the Langmuir isotherm, using the values of K_1, K_2, and Γ_∞ determined in Ref. 17 from the fit of experimental data due to Tajima and coworkers (38, 39) for sodium dodecyl sulfate (SDS). The surface potential $ø_s$ is computed as a function of the surfactant and salt concentrations using steps 2—6 of the calculation procedure described in Sec. 9.2 of Ref. 17 with β = 0. As seen in Fig. 4, E_G increases with the rise in surfactant (SDS) concentration. Moreover, for a fixed surfactant concentration one observes a strong increase in E_G with increase in NaCl concentration. To understand this behavior of E_G we notice that, according to Table 2, E_G depends explicitly only on Γ_1 at fixed temperature T. Hence, the influence of surfactant and salt on the Gibbs elasticity E_G can be interpreted as an increase in the surfactant adsorption Γ_1 with the rise in both surfactant and salt concentrations.

B. Characteristic Time of Adsorption

1. Nonionic Surfactant Solutions

The characteristic time of surfactant adsorption at a fluid interface is an important parameter for surfactant-stabilized dynamic systems such as emulsions. Sutherland (22) derived an expression describing the relaxation of a *small* dilatation of an initially equilibrium adsorption monolayer

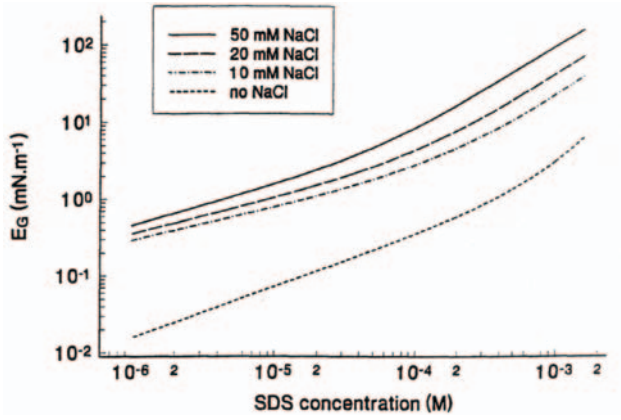

Figure 5 Plot of the Giibs (surface) elasticity E_G vs. the surfactant (SDS) concentration, $c_{1\infty}$. The four curves correspond to four fixed NaCl concentrations: 0, 20, 50, and 115 mM; E_G is calculated by means of Eq. (22) using paraameters values determined from the best fit of experimental data in Ref. 17.

from soluble *nonionic* surfactant (diffusion control):

$$\frac{\sigma(t)-\sigma^{(e)}}{\sigma(0)-\sigma^{(e)}}=\frac{\Gamma_1(t)-\Gamma_1{}^{(e)}}{\Gamma_1(0)-\Gamma_1{}^{(e)}}=\exp\left[\frac{t}{\tau_1}\right]\operatorname{erfc}\left[\sqrt{\frac{t}{\tau_1}}\right] \tag{23}$$

where t is time,

$$\tau_1 \equiv \frac{1}{D_1}\left[\frac{\partial\Gamma_1}{\partial c_1}\right]^2 \tag{24}$$

is the characteristic relaxation time, and D_1 is the surfactant diffusivity; here and hereafter the superscript "(e)" denotes the equilibrium value of the respective parameter; erfc(x) is the complementary error function (40—42). Using the asymptotics of the latter function for $x \gg 1$ one obtains

$$\frac{\sigma(t)-\sigma^{(e)}}{\sigma(0)-\sigma^{(e)}}=\frac{\Gamma_1(t)-\Gamma_1{}^{(e)}}{\Gamma_1(0)-\Gamma_1{}^{(e)}}=\sqrt{\frac{\tau_1}{\pi t}}+0(t^{-3/2}) \tag{25}$$
$$(t \gg \tau_1, \text{ small perturbation})$$

Equation (25) is often used as a test to verify whether the adsorption process is under diffusion control: data for the dynamic surface tension $\sigma(t)$ are plotted versus $t^{1/2}$ and it is checked if the plot complies with a straight line; the extrapolation of this line to $t^{1/2} \to 0$ is used to determine the equilibrium surface tension $\sigma^{(e)}$ (23, 43).

In the experiment one often deals with *large* initial deviations from equilibrium; for example, such is the case when a new oil-water interface is formed by the breaking of larger emulsion drops during emulsification. In the case of large perturbation there is no general analytical expression for the dynamic surface tension $\sigma(t)$ since the adsorption isotherms (except that of Henry, see Table 1) are nonlinear. In this case one can use either a computer solution (44, 45) or apply the von Karman approximate approach (46, 47). Analytical asymptotic expressions for the long time ($t \gg \tau_1$) relaxation of surface tension of a *nonionic* surfactant solution was obtained by Hansen (48):

$$\sigma(t)-\sigma^{(e)}=(\Gamma_1^{(e)})^2\frac{kT}{c_1{}^{(e)}}\sqrt{\frac{1}{\pi D_1 t}} \qquad (t\to\infty) \tag{26}$$

When deriving Eq. (26), the surfactant adsorption at the initial moment was set to zero, $\Gamma_1(0) = 0$. Equation (26) has been verified, utilized, and generalized by many authors (24,49—53). With the help of Eqs (2), (8), and (24) one can represent Eq. (26) in the following equivalent form:

$$\sigma(t)-\sigma^{(e)}=E_G\sqrt{\frac{\tau_1}{\pi t}}+0(t^{-3/2}) \tag{27}$$
$$(t \gg \tau_1, \text{ large perturbation})$$

where, as usual, E_G denotes Gibbs elasticity. Comparison of Eqs (25) and (27) shows that the relaxation of surface tension is characterized by the *same* relaxation time τ_1, irrespective of whether the interfacial perturbation is large or small. (The same conclusion is valid also for ionic surfactants, see below.) For that reason the relaxation time can be considered as a general kinetic property of the adsorption monolayer (36).

2. Ionic Surfactant Solutions

In the case of *ionic* surfactants the existence of a diffuse EDL essentially influences the kinetics of adsorption. The process of adsorption is accompanied by a progressive increase in the surface-charge density and electric potential. The charged surface repels the incoming surfactant molecules, which results in a deceleration of the adsorption process (54). Theoretical studies on the dynamics of adsorption encounter difficulties with the nonlinear set of partial differential equations, which describes the electrodiffusion process (55).

Another important effect, which adds to the complexity of the problem, is the *adsorption* (*binding*) *of counterions* at the conversely charged surfactant head-groups in the adsorption layer, see Fig. 4. The adsorbed (bound) counterions form the Stern layer, which strongly affects the adsorption kinetics of ionic surfactants insofar as up to 70—90% of the surface electric charge could be neutralized by the bound counterions (17, 56—58). The addition of nonamphiphilic electrolyte (salt) in the solution increases the occupancy of the Stern layer. It turns out that in the case of ionic surfactants (with or without salt) there are two adsorbing species: the surfactant ions and the counter-ions. The adsorption of counterions can be described by means of the Stern isotherm (6, 17, 28). It is worthwhile noting that the counterion binding enhances the adsorption of surfactant (17); formally, this appears as a linear increase in the surfactant adsorption parameter K with the rise in the subsurface concentration of counterions, c_{2s}, see Eq. (21).

In recent papers (35, 36) the problem of the kinetics of adsorption from an ionic surfactant solution has been addressed in its full complexity, including the time evolution of the EDL, the effect of added salt, and the counterion binding. An analytical solution was found only in the asymptotic cases of *small* and *large* initial deviations from

equilibrium and *long* times of adsorption. Thus, generalizations of Eqs (25) and (27) for the case of ionic surfactants was obtained (see below). An interesting result is that the electrostatic interaction leads to the appearance of three distinct characteristic relaxation times, those of surfactant adsorption τ_1, of counterion adsorption (binding) τ_2, and of surface-tension relaxation τ_σ. In particular, the relaxation of surfactant and counterion adsorptions, Γ_1 and Γ_2, under electrodiffusion control, is described by the equation:

$$\frac{\Gamma_i(t) - \Gamma_i^{(e)}}{\Gamma_1(0) - \Gamma_1^{(e)}} = \sqrt{\frac{\tau_i}{\pi t}} + 0(t^{-3/2}) \qquad (t \to \infty, i = 1, 2) \tag{28}$$

where τ_1 and τ_2 are given by a generalized version of Eq. (24), which can be found in Refs 35 and 36 together with the procedure for calculations. The relaxation of interfacial tension of *ionic* surfactant solutions is given again by Eqs (25) and (27), in which τ_1 is to be replaced by τ_σ defined as follows (36):

$$\sqrt{\tau_\sigma} = (1 + w)\sqrt{\tau_1} - w\sqrt{\tau_2} - \frac{2qw\lambda}{\kappa} \tanh \frac{\phi_s^{(e)}}{4} \tag{29}$$

where k is the Debye parameter,

$$\kappa^2 \equiv \frac{4\pi z^2 e^2 \sum_i c_{i\infty}}{\varepsilon kT}; \tag{30}$$

$$w \equiv \frac{2kT\Gamma_1^{(e)}}{E_G} \tanh \frac{\phi_s^{(e)}}{2}, \qquad \lambda = \frac{1 + \zeta\Gamma_2^{(e)}/\Gamma_1^{(e)}}{1 + \zeta}, \zeta = \exp(-\phi_s^{(e)}/2) \tag{31}$$

The latter expression for the parameter λ corresponds to the case of large perturbations; for *small* perturbations one simply has $\lambda \equiv 1$ (36). The computations show that for large perturbations λ is close to 1, and therefore the relaxation time is not sensitive to the magnitude of perturbation.

As an illustration, we show in Fig. 6 the calculated dependence of the relaxation times τ_1, τ_2, and τ_σ on the surfactant concentration. As in Fig 5, we have used the values of K_1, K_2, and Γ_∞ determined in Ref. (17) from the fit of experimental data due to Tajima and coworkers (38, 39) for SDS. All necessary equations and the procedure of calculation are described in Ref. 36 for the case of large perturbations. The range of surfactant and salt concentrations correspond to the *nonmicellar* surfactant solutions studied experimentally in Refs 38 and 39. In Fig. 6a and b one notices the wide range of variation in relaxation times, which is from 2 to 6 orders of magnitude. For example, the relaxation time of surface tension, τ_σ, drops from about 40 s for 10^{-5} M SDS down to $\approx 4 \times 10^{-5}$ s for 10^{-3} M SDS (see Fig. 6a). In addition, one sees that systematically $\tau_2 < \tau_1 < \tau_\sigma$; the difference between these three relaxation times can be greater than one order of magnitude for the lower surfactant concentrations, especially in the case without added electrolyte (Fig. 6b). One can conclude that the terms proportional to w in Eq. (29), which give rise to the difference between τ_1 and τ_σ, play an important role, particularly for solutions of lower ionic strength. Figure 6 demonstrates

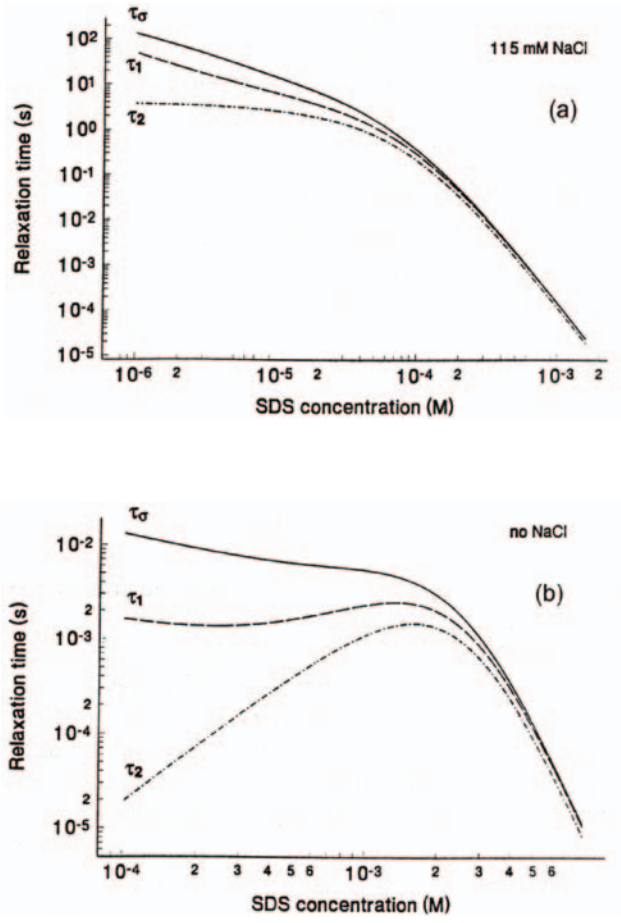

Figure 6 Ionic surfactant solution: relaxation times of interfacial tension. τ_σ, of surfactant adsorption, τ_1, and of counterion adsorption (binding), τ_2, calculated in Ref. 36 as functions of surfactant (SDS) concentration, $c_{1\infty}$, using parameters values determined from the best fit of experimental data in Ref. 17. (a) SDS solutions with 115 mM added NaCl; (b) SDS solutions without added NaCl.

that the approximation $\tau_\sigma \approx \tau_1$, which is widely used in the literature, is applicable only for the higher surfactant concentrations, for which $\tau_\sigma \to \tau_1$. Note also that for a given surfactant concentration τ_2 is always smaller than τ_1 and τ_σ, that is, the adsorption of counter-ions relaxes faster than does the adsorption of surfactant ions and the surface tension.

The physical importance of these results is related to the fact that the coalescence of drops at the early highly dynamic stages of emulsion production is expected to be sensitive to the degree of saturation of the newly created interfaces with surfactant, and correspondingly, to the relaxation time of surfactant adsorption. The surfactant transport is especially important when the emulsion is prepared from nonpre-equilibrated liquid phases. In such cases one can observe dynamic phenomena like the *cyclic dimpling* (59, 60) and *osmotic swelling* (61), which bring about additional stabilization of the emulsions (see also Refs 1 and 62).

3. Micellar Surfactant Solutions

Emulsions are often prepared from micellar surfactant solutions. As known, above a given critical micelle concentration (cmc) surfactant aggregates (micelles) appear inside the surfactant solutions. At rest the micelles exist in equilibrium with the surfactants monomers in the solution. If the concentration of the monomers in the solution is suddenly decreased, the micelles release monomers until the equilibrium concentration, equal to cmc, is restored at the cost of disassembly of a part of the micelles (63, 64).

The dilatation of the surfactant adsorption layer leads to a transfer of monomers from the subsurface to the surface, which causes a transient decrease in the subsurface concentration of monomers. The latter is compensated for by disintegration of a part of the micelles in the subsurface layer. This process is accompanied by a diffusion transport of surfactant monomers and micelles due to the appearance of concentration gradients. In general, the micelles serve as a powerful source of monomers which is able to saturate quickly the surface of the newly created emulsion drops. In this way, the presence of surfactant micelles strongly accelerates the kinetics of adsorption.

The theoretical model developed by Aniansson and coworkers (65-68) describes the micelles as polydisperse aggregates, whose growth or decay happens by exchange of monomers. The general theoretical description of the diffusion in such a solution of polydisperse aggregates taking part in chemical reactions (exchange of monomers) is a heavy task; nevertheless, it has been addressed in several works (69—72). The relaxation of surface tension of a micellar solution at small initial deviation from equilibrium can be described by the following expression, derived in Ref. 70:

$$\frac{\sigma(t)-\sigma^{(e)}}{\sigma(0)-\sigma^{(e)}} = \frac{\Gamma_1(t)-\Gamma_1^{(e)}}{\Gamma_1(0)-\Gamma_1^{(e)}} = \frac{1}{g_1-g_2}[E(g_1,\tau)-E(g_2,\tau)]\exp\left[-\frac{t}{\tau_m}\right] \tag{32}$$

$$E(g,\tau) = g\exp(g^2\tau)\operatorname{erfc}(g\sqrt{\tau})$$
$$\tau = t/\tau d$$
$$g_{1,2} = [1 \pm \sqrt{1+4\tau_d/\tau_m}]/2$$
$$\tau_m = [K_d(1+m^2 c_m^{(e)}/c_1^{(e)})]^{-1}$$
$$\tau_d = (\partial\Gamma_1/\partial c_1)^2/D_1 \tag{33}$$

where τ_m and τ_d are the characteristic relaxation times of micellization and monomer diffusion (see Ref. 73). For the sake of estimates τ_d can be identified with τ_1 as given by Eq. (24); K_d is the rate constant of micelle decay; as earlier, the index "(e)" refers to the equilibrium state; and m is the average micelle aggregation number. In the absence of micelles $\tau_d/\tau_m \to 0$; then, $g_1 = 1$, $g_2 = 0$, and Eq. (32) reduces to Eq. (23), as should be expected. One can estimate the characteristic time of relaxation in the presence of micelles by using the following combined expression:

$$\tau_\sigma \approx \frac{4\tau_d}{(1+\sqrt{1+4\tau_d/\tau_m})^2} \tag{34}$$

According to the latter $\tau\sigma$ expression $\tau_\sigma \approx \tau_m$ for $\tau_d \gg \tau_m$, and $\tau_\sigma \approx \tau_d$ for $\tau_d \ll \tau_m$.

Equation (32) is applicable only for small perturbations. An approximate analytical approach, which is applicable for both small and large deviations from equilibrium, is developed in Ref. 47.

III. MECHANISMS OF COALESCENCE

A. Mechanisms of Rupture of Emulsion Films

1. Thermodynamic and Kinetic Factors Preventing Coalescence

Often the contact of two emulsion drops is accompanied by the formation of a liquid film between them. The rupture of this film is equivalent to coalescence of the drops, that is,

step D→C in Fig 2. Figure 7 shows schematically the zone of contact between two emulsion drops of different radii, R_1 and R_2 ($R_1 < R_2$). For the sake of simplicity we assume that the two drops are composed of the same liquid and have the same surface tension σ. The film formed in the contact zone has radius R and thickness h. The interaction of the two drops across the film leads to the appearance of an additional *disjoining pressure* Π inside the film, which in general depends on the film thickness: Π = Π (h) (see, e.g., Refs 2—4 and 62). Positive Π corresponds to repulsion between the two film surfaces (and the two drops), whereas negative Π corresponds to attraction between them. The presence of a disjoining pressure gives rise to a difference between the tension of the film surfaces, σ^f, and the interfacial tension σ of the droplets. The force balance at the contact line reads (62, 74, 75):

$$\sigma^f = \sigma \cos \alpha; \tag{35}$$

where a is the contact angle, which is related to the disjoining pressure n as follows (62, 76):

$$\cos \alpha = 1 + \frac{1}{2\sigma} \int_h^\infty \Pi(h)\, dh \tag{36}$$

Since cos α < 1, a necessary condition to have a contact angle is for the integral in Eq. (36) to be negative; for emulsion drops this can be ensured by the longrange van der Waals attraction, which dominates Π for the larger h (see Fig. 8a). Geometrically, α appears as the angle subtended between the tangents to the film and drop surfaces at the contact line (Fig. 7). At *equilibrium* (no applied external force) the radius of the film between the two drops is determined by the equation:

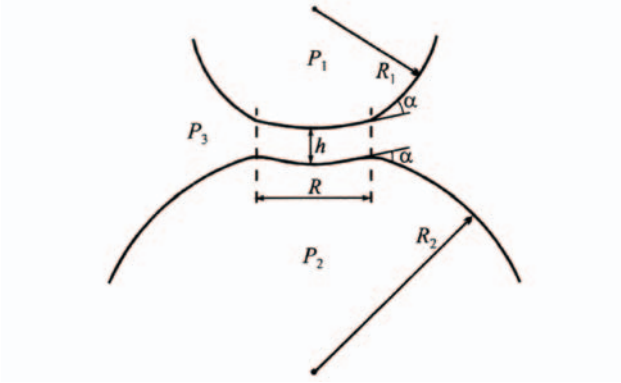

Figure 7 Sketch of a film between two nonidentical emulsion drops of radii R_1 and R_2. The film thickness and radius are denoted by h and R, respectively; α is the contact angle, and P_1, P_2, and P_3 denote the pressure in the respective liquid phases.

$$R = \frac{2\sigma \sin \alpha}{\Pi} \cos \theta \approx \frac{2\sigma \sin \alpha}{\Pi}; \qquad \cos \theta \equiv (1 - R^2/R_f^2)^{1/2} \approx 1 \tag{37}$$

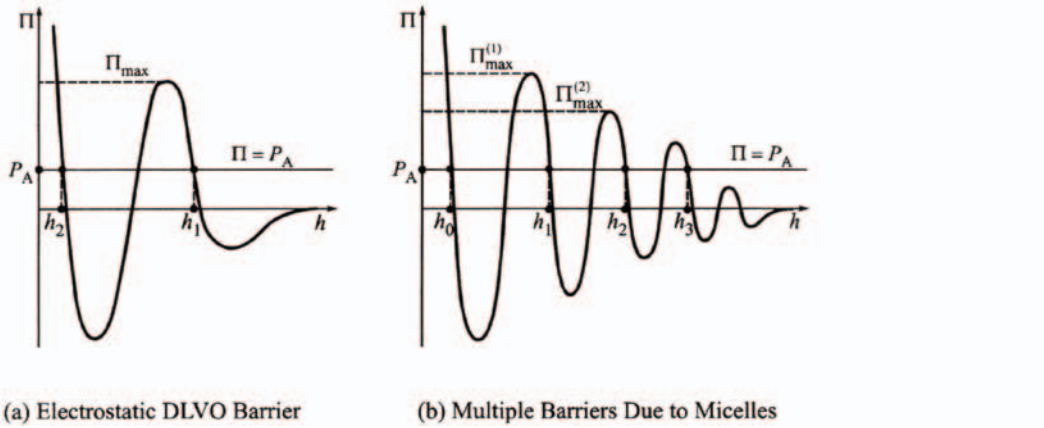

Figure 8 Typical plots of disjoining pressure Π vs. film thickness h; P_A is the pressure difference applied across the film surface, see Eq (43); the equilibrium states of the liquid film correspond to the points in which Π = P_A. (a) DLVO-type disjoining-pressure isotherm Π (h); the points at $h = h_1$ and h_2 correspond to primary and secondary films, respectively; Π_{max} is the height of a barrier resulting from the electrostatic repulsion between the film surfaces, (b) Oscillatory structural force between the two film surfaces caused by the presence of surfactant micelles (or other monodisperse colloidal particles) in the continuous phase; Π (h) exhibits multiple decaying oscillations; the stable equilibrium films with thickness h_0, h_1, h_2, and h_3 corresponds to stratifying films containing 0, 1, 2, and 3 layers of micelles, respectively (see Fig. 9).

where R_f is the curvature radius of the film. Equation (37) follows from Eqs (144) and (179) in Ref. 75. One sees that the greater the contact angle α, the larger the equilibrium film radius R. On the other hand, for α = 0 the equilibrium film radius R is also zero and there are no equilibrium doublets or larger aggregates (flocs) of emulsion droplets.

If the two drops have different radii, as in Fig. 7, the film between them is curved. The balance of the pressures applied per unit area of the two film surfaces can be expressed by means of versions of the Laplace equation (75):

$$\frac{2\sigma^f}{R_f} = P_1 - (P_3 + \Pi) \qquad \text{(upper film surface)} \quad (38)$$

$$\frac{2\sigma^f}{R_f} = (P_3 + \Pi) - P_2 \qquad \text{(lower film surface)} \quad (39)$$

where P_1 and P_2 are the pressures inside the respective drops (Fig. 7), and P_3 is the pressure in the continuous phase; the effect of disjoining pressure is equivalent to an increase in the pressure within the film, which is $P_3 + \Pi$. To obtain Eqs (38) and (39) we have neglected some very small terms, of the order of h/R_f (see Ref. 75 for details). To determine R_f we apply the Laplace equations for the two drops (Fig. 7):

$$\frac{2\sigma}{R_1} = P_1 - P_3, \qquad \frac{2\sigma}{R_2} = P_2 - P_3 \qquad (40)$$

Combining Eqs (36) and (38)-(40) one determines the curvature radius of the film:

$$\frac{1}{R_f} = \frac{1}{2\cos\alpha}\left(\frac{1}{R_1} - \frac{1}{R_2}\right) \qquad (41)$$

If the two drops have identical size ($R_1 = R_2$), then Eq. (41) yields $1/R_f \to 0$, i.e., the film between the drops is flat, as should be expected.

The disjoining pressure n is the major *thermodynamic* stabilizing factor against drop coalescence. A stable equilibrium state of a liquid film can exist only if the following two conditions are satisfied (3):

$$\Pi = P_A \qquad \text{and} \qquad \left(\frac{\partial \Pi}{\partial h}\right)_{\Pi = P_A} < 0 \qquad (42)$$

Here, P_A is the pressure difference applied across the surface of the film, which in view of Eqs (38) and (39) can be expressed in the form:

$$P_A = P_1 - P_3 - \frac{2\sigma^f}{R_f} = \frac{2\sigma^f}{R_f} + P_2 - P_3 = \sigma\left(\frac{1}{R_1} + \frac{1}{R_2}\right) \qquad (43)$$

At the last step we have used also Eqs (35), (40), and (41). For two identical drops $R_f \to \infty$, and then P_A reduces to the capillary pressure of the drops: $P_A = 2\sigma/R_1 = 2\sigma/R_2$. The condition $\Pi = P_A$, see Eq. (42), means that at equilibrium the disjoining pressure Π counterbalances the pressure difference P_A applied across the film surface. In addition, the condition $\partial\Pi/\partial h < 0$ guarantees that the equilibrium is *stable* (rather than unstable).

As an illustration, Fig. 8a shows a typical DLVO-type disjoining-pressure isotherm $\Pi(h)$ (see Refs 3, 4 and 62 for more details). There are two points, $h = h_1$ and $h = h_2$, at which the condition for stable equilibrium, Eq. (42), is satisfied. In particular, $h = h_1$ corresponds to the so-called *primary film*, which is stabilized by the electrostatic (double layer) repulsion. The addition of electrolyte to the solution may lead to a decrease in the height of the electrostatic barrier, Π_{max} (3,4); at high electrolyte concentration it is possible to have $\Pi_{max} < P_A$, then the primary film does not exist. Note, however, that the increase in electrolyte concentration may lead also to a shift in the maximum toward smaller thicknesses and to an increase in the barrier Π_{max}. Therefore, primary films could be observed even at relatively high salt concentrations.

The equilibrium state at $h = h_2$ (Fig. 8a) corresponds to a very thin *secondary film*, which is stabilized by the short-range Born repulsion. The secondary film represents a bilayer of two adjacent surfactant mono-layers; its thickness is usually about 5 nm (slightly greater than the doubled length of the surfactant molecule) (77). Secondary films can be observed in emulsion floes and in creamed emulsions.

The situation is more complicated when the aqueous solution contains surfactant micelles, which is a common experimental and practical situation. In such a case the disjoining pressure isotherm $\Pi(h)$ can exhibit multiple decaying oscillations, whose period is close to the diameter of the micelles (Fig. 8b) (for details see, e.g., Ref. 78). The condition for equilibrium liquid film, Eq. (42), can be satisfied at several points, denoted by h_0, h_1, h_2, and h_3 in Fig. 8b; the corresponding films contain 0, 1,2, and 3 layers of micelles, respectively. The transitions between these multiple equilibrium states represent the phenomenon *stratification* (see Fig. 9 and Refs 78-91). The presence of dis-

joiningpressure barriers, which result from either the electrostatic repulsion (Fig. 8a) or the oscillatory structural forces (Fig. 8b), has a stabilizing effect on liquid films and emulsions (2).

The existence of a stable equilibrium state (see Fig. 8) does not guarantee that a draining liquid film can "safely" reach this state. Indeed, hydrodynamic instabilities, accompanying the drainage of liquid, could rupture the film before it has reached its thermodynamic equilibrium state (1). There are several *kinetic stabilizing factors*, which suppress the hydrodynamic instabilities and decelerate the drainage of the film, thus increasing its lifetime. Such a factor is the *Gibbs* (*surface*) *elasticity*, E_G, of the surfactant adsorption mono layers (see Sec. II. A); it tends to eliminate the gradients in adsorption and surface tension and damps the fluctuation capillary waves. At higher surfactant and salt concentrations the Gibbs elasticity is also higher and it renders the interface tangentially immobile (see Fig. 5). The *surface viscosity* also impedes the drainage of water out of the films because of the dissipation of a part of the kinetic energy of the flow within the surfactant adsorption monolayers (see Sec. IV). The *surfactant adsorption relaxation time* (see Sec. II.B) is another important kinetic factor. If the adsorption relaxation time is short enough, a dense adsorption monolayer will cover the newly formed emulsion drops during the emulsification and will protect them against coalescence upon collision. In the opposite case (slow adsorption kinetics) the drops can merge upon collision and the emulsion will be rather unstable.

2. Mechanism of Film Breakage

The role of the emulsion stabilizing (or destabilizing) factors can be understood if the mechanism of film breakage is known. Several different mechanisms of rupture of liquid films have been proposed, which are briefly described below.

The *capillary-wave mechanism* has been proposed by de Vries (92) and extended in subsequent studies (2, 24, 93—98) (see Fig. 10a). The conventional version of this mechanism is developed for the case of monotonic attraction between the two surfaces of a liquid film (say, van der Waals attraction). Thermally excited fluctuation capillary waves are always present at the film surfaces. With the decrease in average film thickness, h, the attractive disjoining pressure enhances the amplitude of some modes of the fluctuation waves. At a given critical value of the film thickness, h_c, corrugations on the two opposite film surfaces can touch each other and then the film will break (97). The same mechanism takes place also in the case of slightly deformed emulsion drops. If the emulsion drops are quiescent, only the thermodynamic and geometric factors determine the critical thickness; indeed, the finite area of the drops (films) imposes limitation on the maximum length of the capillary waves (see Secs III.B and III.C). When the breakage happens during the drainage of the emulsion film (during the approach of the emulsion drops), then the critical thickness is also affected by various hydrodynamic factors (see Sec. IV for details).

The mechanism of *film rupture by nucleation of pores* has been proposed by Derjaguin and Gutop (99) to explain the breaking of very thin films, built up from two attached monolayers of amphiphilic molecules. Such are the secondary foam and emulsion films and the bilayer lipid membranes. This mechanism was further developed by Derjaguin and Prokhorov (3, 100, 101), Kashchiev and Exerowa (102—104), Chizmadzhev and coworkers (105—107), and Kabalnov and Wennerström (108). The formation

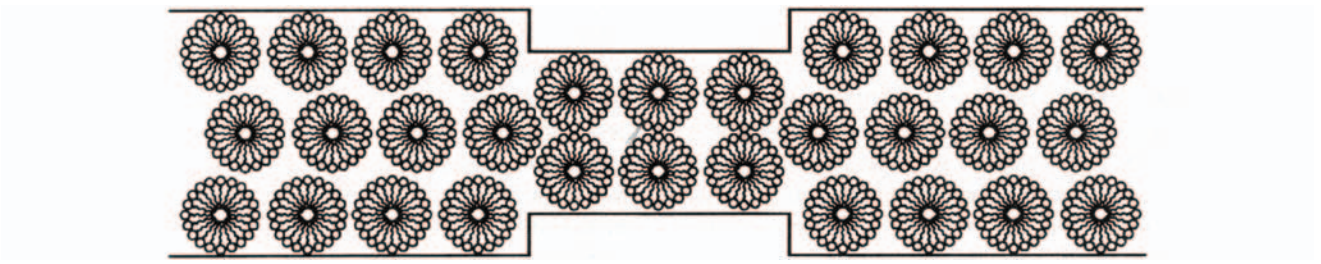

Figure 9 The spot of lower thickness in a stratifying liquid film corresponds to a local decrease in the number of micelle layers in the colloid-crystal-like structure of surfactant micelles formed inside the liquid film. The appearance of spots could be attributed to the condensation of vacancies in that structure. (From Ref. 82.)

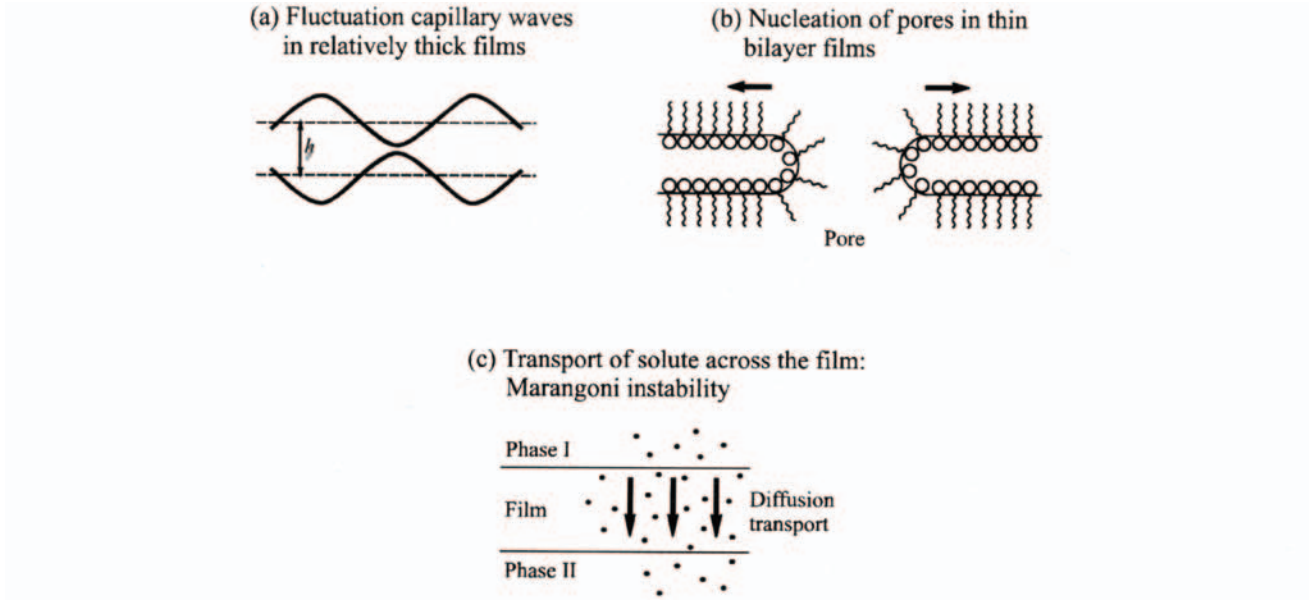

Figure 10 Mechanisms of breakage of liquid films, (a) *Fluctuation-wave-mechanism*: the film rupture results from growth of capillary waves enhanced by attractive surface forces (92). (b) *Pore-nudeation mechanism*: it is expected to be operative in very thin films, virtually representing two attached monolayers of amphiphilic molecules (99). (c) *Solute-transport mechanism*: if a solute is transferred across the two surfaces of the liquid film due to gradients in the solute chemical potential, then Marangoni instability could appear and break the film (109).

of a nucleus of a pore (Fig. 10b) is favored by the decrease in surface energy, but it is opposed by the edge energy of the pore periphery. The edge energy can be described (macroscopically) as a line tension (100—104) or (micromechanically) as an effect of the spontaneous curvature and bending elasticity of the amphiphilic monolayer (108). For small nuclei the edge energy is predominant, whereas for larger nuclei the surface energy gets the upper hand. Consequently, the energy of pore nucleation exhibits a maximum at a given *critical* pore size; the larger pores spontaneously grow and break the film, while the smaller pores shrink and disappear.

A third mechanism of liquid-film breakage is observed when there is a *transport of solute across the film* (see Fig. 10c). This mechanism, investigated experimentally and theoretically by Ivanov and coworkers (109—111), was observed with emulsion systems (transfer of alcohols, acetic acid, and acetone across liquid films), but it could appear also in some asymmetric oil-water-air films. The diffusion transport of some solute across the film leads to the development of Marangoni instability, which manifests itself as a forced growth of capillary waves at the film surfaces and eventual film rupture. Note that Marangoni instability can be caused by both mass and heat transfer (112—114).

A fourth mechanism of film rupture is the *barrier mechanism*. It is directly related to the physical interpretation of the equilibrium states depicted in Fig. 8. For example, let us consider an electrostatically stabilized film of thickness h_1 (Fig. 8a). Some processes in the system may lead to an increase in the applied capillary pressure P_A. For instance, if the height of the column of an emulsion cream increases from 1 to 10 cm, the capillary pressure in the upper part of the cream increases from 98 to 980 Pa owing to the hydrostatic effect. Thus, P_A could become greater than the height of the barrier, Π_{max}, which would cause either film rupture (and coalescence) or transition to the stable state of secondary film at $h = h_2$ (Fig. 8a). The increase in the surfactant adsorption density stabilizes the secondary films. In addition, the decrease in Π_{max} decreases the probability of the film rupturing after the barrier is overcome. Indeed, the overcoming of the barrier is accompanied by a violent release of mechanical energy accumulated during the increase

in P_A. If the barrier is high enough, the released energy could break the liquid film. On the other hand, if the barrier is not too high, the film could survive the transition.

The overcoming of the barrier can be facilitated by various factors. Often the transition happens through the formation and expansion of spots of lower thickness within the film, rather than by a sudden decrease in the thickness of the *whole* film. Physically this is accomplished by a nucleation of spots of submicrometer size, which resembles a transition with a "tunnel effect," rather than a real overcoming of the barrier. A theoretical model of spot formation in stratifying films by condensation of vacancies in the structure of ordered micelles (vacancy mechanism) has been developed in Ref. 82 (see Figs 8b and 9). The nucleation of spots makes the transitions less violent and decreases the probability of film breakage. The increase in applied capillary pressure P_A facilitates spot formation and the transition to a state with lower film thickness; this has been established by Bergeron and Radke (85), who experimentally obtained portions of the stable branches of the oscillatory disjoining-pressure curve (Fig. 8b) for foam films. Oscillatory disjoining-pressure curves resulting from reverse micelles in an oily phase were directly measured by Parker et al. (86) by using a version of the surface-force apparatus. Marinova et al. (91) investigated the stabilizing role of the oscillatory disjoining pressure in oil-in-water emulsions which contained surfactant micelles in the aqueous phase.

Below we present in more detail the predictions of the capillary-wave mechanism.

B. Critical Thickness of Quiescent Emulsion Films

Let us first consider a quiescent emulsion film, say the film between two drops within a floc or cream. At a given sufficiently small thickness of the film, termed the *critical thickness* (92—97, 115), the attractive surface forces prevails and causes growth of the thermally excited capillary waves. This may lead to either film rupture or transition to a thinner secondary film. Two modes of film undulation have been distinguished: symmetric (squeezing, peristaltic) and antisymmetric (bending) modes; it is the symmetric mode which is related to the film breakage/transition. The critical thickness, $h = h_c$, of a film having area πR^2 can be estimated from the equation (94):

$$\frac{2R^2}{\sigma}\left(\frac{\partial \Pi}{\partial h}\right)_{h=h_c} = j_1^2 = 5.783\ldots, \qquad (44)$$

where j_1 is the first zero of the Bessel function j_0; as usual, σ denotes surface tension. Equation (44) has been derived in a different manner by Vrij (94), Ivanov et al. (95), and Malhotra and Wasan (116). It is obvious that Eq. (44) can be satisfied only for positive $\partial\Pi/\partial h$. If, in the special case of van der Waals interaction one is to substitute $\partial\Pi/\partial h$ by $A_H/(2\pi h^4)$, where A_H is the Hamaker constant, then from Eq. (44) it follows that the critical thickness increases with increase in the film radius R, i.e., the films of larger area break more easily (at a greater thickness) than those of smaller area. Note that the effect of surfactant on the tangential mobility of the interface, which involves the surface elasticity, viscosity, and diffusion, does not affect the form of Eq. (44), and correspondingly, the critical thickness h_c. The surfactant affects Eq. (44) and h_c only indirectly, through the values of σ and $\partial\Pi/\partial h$. These conclusions are valid only for quiescent films, which do not thin during the development of instability.

When an aqueous film is stabilized by an ionic surfactant, then the stability problem becomes more complicated owing to the electrostatic interactions between the charged film surfaces (117). Electrolyte films surrounded by dielectric were initially studied by Felderhof (118), who examined the stability of an equilibrium infinite plane-parallel film surrounded by a vacuum. Sche and Fijnaut (119) extended Felderhof s analysis to account for the effect of surface shear viscosity and surface elasticity. In these studies the electrostatic (double-layer) component of disjoining pressure Π was involved in the theory, and a quasistatic approximation was used to describe the electrostatic interaction (117—119). In other words, it has been assumed that the ions immediately acquire their equilibrium distribution for each instantaneous shape of the film. The electric field has been computed by solving the Poisson - Boltzmann equation for the respective instantaneous charge configuration. This quasistatic approximation, which neglects the electrodiffusion fluxes, leads to a counterpart of Eq. (44) in which the total disjoining pressure Π includes an electrostatic component. The latter leads to $\partial\Pi/\partial h < 0$ at the equilibrium state ($h = h_1$ in Fig. 8a) and then Eq. (44) has no positive root for $h = h_c$; that is, the film should remain stable for an infinitely long time in agreement with the conventional DLVO theory (3). On the other hand, if electrolyte is added at sufficiently high concentration, the double-layer repulsion is suppressed and the liquid films rupture under the action of the van der Waals force [see Ref. 120 and Eq. (86)].

In reality, aqueous films stabilized with ionic surfactant, without electrolyte, also rupture, especially at surfactant concentrations below the cmc. The latter fact cannot be explained in the framework of the quasistatic approximation (117—119); this is still an open problem in the theory of liquid-film stability.

C. Critical Distance Between Quiescent Emulsion Drops

Let us consider two emulsion drops of different radii, R_1 and R_2, like those depicted in Fig. 7 but without the formation of a film between them, i.e., $R = 0$. In this case the gap between the two drops represents a liquid film of uneven thickness. The frequently used lubrication approximation (121) is not applicable to a description of the fluctuation capillary waves on the drop surfaces because it presumes infinite interfacial area and does not impose the natural upper limits on the capillary wavelength, originating from the finite size of the drops. On the other hand, it is possible to solve the problem by means of the usual spherical coordinates, locating the co-ordinate origin at the center of one of the two drops. We consider the case in which effects of surface electric charge are negligible and the interaction between the drops (the disjoining pressure) is dominated by the van der Waals attraction. The critical distance between the two drops can be determined from a thermodynamic requirement, viz., the fluctuation of the local disjoining pressure in the narrowest zone of the gap to be equal to the fluctuation of the capillary pressure of the drops. (For shorter distance the fluctuation of the attractive disjoining pressure will prevail and will initiate film rupture.) This requirement leads to the following equation:

$$\frac{1}{\sin\theta}\frac{d}{d\theta}\left[\sin\theta\,\frac{d\zeta}{d\theta}\right] + \left\{2 + \frac{A_{\mathrm{H}}\,a^2\cos^2\theta}{\pi\sigma}\,[h + 2a(1-\cos\theta)]^{-4}\right\}\zeta = 0, \tag{45}$$

Here, ζ is the fluctuation in the drop shape, θ is the polar angle of the spherical coordinate system, h is the shortest distance between the two drop surfaces, A_H is the Hamaker constant and

$$a = 2R_1R_2/(R_1 + R_2) \tag{46}$$

is the mean drop radius. We used the following two boundary conditions: (1) $d\zeta/d\theta = 0$ at $\theta = 0$, i.e., at the narrowest region of the gap; and (2) $\zeta = 0$ for $\theta = \pi/2$, that is, far from the gap zone. The value $h = h_c$, corresponding to the *greatest* eigenvalue of the spectral problem, Eq. (45), gives the critical distance between the two drops. Note that the effect of surfactant on the tangential mobility of the interface, which involves the surface elasticity, viscosity, and diffusion, does not affect the form of Eq. (45), and correspondingly, the critical distance h_c. We found the greatest eigenvalue numerically. The results for the critical distance as a function of the drop radius a and the Hamaker constant A_H are shown in Fig. 11; for the interfacial tension we used the value $\sigma = 30$ mN/m. One sees that the critical distance is of the order of dozens of nanometers and that it increases with the rise of both A_H and a.

Note, however, that if the two drops are not quiescent, but instead approach each other, the critical distance is influenced by the hydrodynamic interactions —- see the next section.

IV. HYDRODYNAMIC INTERACTIONS AND DROP COALESCENCE

First, we consider the hydrodynamic interactions between two emulsion drops, which remain spherical when the distance between them decreases (Sec. IV.A); this is the transition A→B in Fig. 2. Second, we consider the thinning of the film formed between two emulsion drops (Sec. IV.B): this is stage D in Fig. 2. In both cases the effect of surfactant is taken into account and the critical distance (thickness) for drop coalescence is quantified.

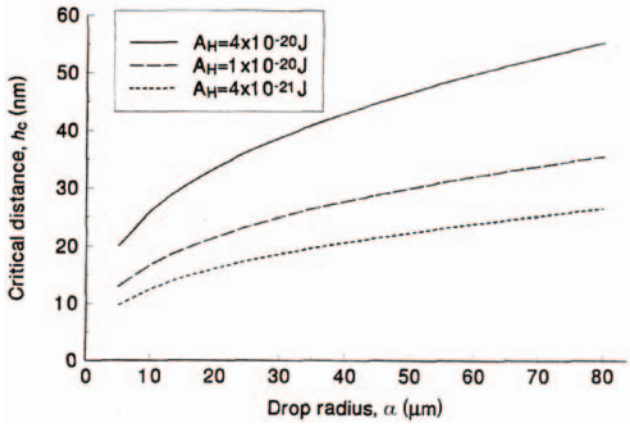

Figure 11 Plot of the critical distance between two quiescent drops, h_c, vs the mean drop radius, a, calculated by means of Eq. (45) for three values of the Hamaker constant A_H.

A. Interaction of Spherical Emulsion Drops

1. Limiting Cases of Low and High Surface Mobility

The solution to the problem of hydrodynamic interaction between two rigid spherical particles, approaching each other across a viscous fluid, was obtained by Taylor (122). Two spherical emulsion drops of *tangentially immobile* surfaces (due to the presence of dense surfactant adsorption monolayers) are hydrodynamically equivalent to the two rigid particles considered by Taylor. The hydrodynamic interaction is due to the dissipation of kinetic energy when the liquid is expelled from the gap between the two spheres. The resulting friction force decreases the velocity of the two spherical drops proportionally to the decrease in the surface-to-surface distance h in accordance with the Taylor (122) equation:

$$V_{\mathrm{Ta}} = \frac{2h}{3\pi\eta a^2}(F - F_s) \quad \text{(tangentially immobile surfaces)} \tag{47}$$

Here, a is the mean drop radius denned by Eq. (46), F is the external force exerted on each drop, and F_s is the surface force originating from the intermolecular interactions between the two drops across the liquid medium. When the range of the latter interactions is much smaller than the drop radii, then F_s can be calculated by means of the Derjaguin approximation (3, 4):

$$F_s = \pi a \int_h^\infty \Pi(h)\, dh \tag{48}$$

where, as before, Π is the disjoining pressure.

If the surface of an emulsion drop is mobile, it can transmit the motion of the outer fluid to the fluid within the drop. This leads to a circulation of the fluid inside the drop and influences the dissipation of energy in the system. The problem about the approach of two nondeformed spherical drops or bubbles in the *absence of surfactants* has been investigated by many authors (123-132). A number of solutions, generalizing the Taylor equation [Eq. (47)], have been obtained. In particular, the velocity of central approach of two spherical drops in pure liquid, V_{p}, is related to the Taylor velocity V_{Ta}, defined by means of a Padé-type expression derived by Davis et al. (131):

$$\xi \equiv \frac{\eta_{out}}{\eta_{in}}\sqrt{\frac{a}{2h}} \tag{50}$$

where, as usual, h is the closest surface-to-surface distance between the two drops, and η_{in} and η_{out} are the viscosities of the liquids inside and outside the drops. In the limiting case of solid particles one has $\eta_{in} \leqq \infty$, $\xi \to 0$ and then Eq. (49) reduces to the Taylor equation, Eq. (47). Note that in the case of a *close* approach of two drops ($h \to 0$, $\xi \gg 1$) the velocity V_{p} is proportional to $h^{1/2}$. This implies that the two drops can come into contact ($h = 0$) in a finite period of time ($\tau < \infty$) under the action of a given force, F, because the integral expressing the lifetime (97):

$$\tau = \int_{h_c}^{h_{in}} \frac{dh}{V} \tag{51}$$

(with $V = V_{\mathrm{p}}$) is convergent for $h_c = 0$; h_{in} is the surface-to-surface distance at the initial moment $t = 0$. In contrast, in the case of immobile interfaces ($\xi \ll 1$) Eq. (47) gives $V_{\mathrm{Ta}} \propto h$ and $\tau \to \infty$ for $h_c \to 0$. Moreover, the counterbalancing of the external force by the surface force, i.e., $F - F_s = 0$, implies $V_{\mathrm{Ta}} = V = 0$ and $\tau \to \infty$ (equilibrium state) irrespective of whether the drop surfaces are tangentially mobile or immobile.

It has been established both theoretically and experimentally (133, 134) that, if the surfactant is dissolved only in the drop phase, the film formed between two emulsion drops (Fig. 2D) thins just as if surfactant is missing. Likewise, one can use Eq. (49) to estimate the velocity of approach of two emulsion drops when surfactant is contained only in the drop phase (2).

2. Effects of Surface Elasticity, Viscosity, and Diffusivity

When surfactant is present in the continuous phase at not too high concentration, then the surfactant adsorption monolayers, covering the emulsion drops, are tangentially mobile, rather than immobile. The adsorbed surfactant can be dragged along by the fluid flow in the gap between two colliding drops, thus affecting the hydrodynamic interaction between them. The appearance of gradients of surfactant adsorption are opposed by the Gibbs elasticity, surface viscosity, and surface and bulk diffusion. Below, we consider the role of the enumerated factors on the velocity of approach of two emulsion drops.

If the driving force F (say, the Brownian or the buoyancy force) is small compared to the capillary pressure of the

droplets, the deformation of two spherical droplets upon collision will be only a small perturbation in the zone of contact. The film thickness and the pressure within the gap can then be presented as a sum of a nonperturbed part and a small perturbation. Solving the resulting hydrodynamic problem for low (negligible) interfacial viscosity, an analytical formula for the velocity of drop approaching, $V = -dh/dt$, can be derived (121):

$$\frac{V}{V_{\mathrm{Ta}}} = \frac{h_s}{2h}\left[\frac{d/h+1}{d/h}\ln(d/h+1) - 1\right]^{-1} \tag{52}$$

where a is the mean drop radius denned by Eq. (46), and V_{Ta} is the Taylor velocity, Eq. (47); the other parameters are defined as follows:

$$d \equiv \frac{h_s}{1+b} \tag{53}$$

$$h_s \equiv \frac{6\eta_{out} D_{1,s}}{E_G} \tag{54}$$

$$b \equiv \frac{3\eta_{out} D_1}{E_G}\left(\frac{\partial c_1}{\partial \Gamma_1}\right)^{(e)} = \frac{3\eta_{out} D_1}{\Gamma_1^{(e)}}\left(\frac{\partial c_1}{\partial \sigma}\right)^{(e)} \tag{55}$$

As usual, the superscript (e) denotes that the respective quantity should be estimated for the equilibrium state; the dimensionless parameter b accounts for the effect of *bulk diffusion*, whereas h_s has a dimension of length and takes into account the effect of *surface diffusion*. In the limiting case of very large *Gibbs elasticity* E_G (tangentially immobile interface) the parameter d tends to zero and then Eq. (52) yields $V \to V_{\mathrm{Ta}}$, as should be expected (121, 135, 136).

If the effect of *surface viscosity* is taken into account, then Eq. (52) can be expressed in the generalized form (137, 138):

$$\frac{V}{V_{\mathrm{Ta}}} = \Phi_{\mathrm{v}}(h; h_s, d, s_{\mathrm{v}}) \tag{56}$$

where Φ_{V} is termed the *mobility factor* (*function*); the dimensionless parameter S_{V} takes into account the effect of surface viscosity:

$$s_{\mathrm{v}} \equiv \frac{\eta_s}{6a\,\eta_{out}}, \qquad \eta_s \equiv \eta_{\mathrm{sh}} + \eta_{\mathrm{dil}} \tag{57}$$

Here, η_{sh} and η_{dil} respectively, the interfacial shear and dilatational viscosities. In fact, Eq. (52) gives an analytical expression for the mobility factor Φ_{V} in the case when $S_{\mathrm{V}} \ll 1$, i.e., the effect of surface viscosity can be neglected. However, if the effect of surface viscosity is essential, there is no analytical expression for Φ_{V}; in this case a numerical procedure for computation of Φ_{V} has been developed (137, 138). Table 3 contains asymptotic expressions for Φ_{V}. A general property of Φ_{V} is

Table 3 Asymptotic Expressions for Mobility Factors

Asymptotic cases	Mobility factors (Φ_{v} and Φ_{p})
$\frac{d}{h} \ll 1$	$\Phi_{\mathrm{v}} = (b+1)/\left[1 - \frac{d}{3h} + \frac{8s_{\mathrm{v}}b}{3(b+1)}\left(b + \frac{d}{h}\right)\right]$
	$\Phi_{\mathrm{p}} = \frac{\Phi_{\mathrm{v}}}{b+1}\left[1 - \frac{2d}{3h} + \frac{16s_{\mathrm{v}}b}{3(b+1)}\left(b + \frac{2d}{h}\right)\right]$
$\frac{d}{h} \gg 1$	$\Phi_{\mathrm{v}} = \frac{h_s}{2h}/\left[\frac{4s_{\mathrm{v}}h_s}{3h} - 1 - 8s_{\mathrm{v}} + 1n\frac{d}{h}\right]$
	$\Phi_{\mathrm{p}} = \frac{2h\Phi_{\mathrm{v}}}{h_s}\left(\frac{1+8s_{\mathrm{v}}h_s}{3h}\right)$

Source: Ref. 138.

$$\Phi_{\mathrm{v}} = 1 \quad \text{for} \quad E_G \to \infty \quad \text{(tangentially immobile surfaces)} \tag{58}$$

It is important to note that the surface viscosity parameter S_{V} appears only in the combinations $S_{\mathrm{V}}h_s/h = \eta_s D_{1s}/(hE_G a)$ and $S_{\mathrm{V}}b$ (see Table 3). In view of Eqs (53)-(55), it then follows that the surface viscosity can influence the mobility factor Φ_{V} only if either the Gibbs elasticity, E_G, or the drop radius, a, or the gap width, h, are small enough.

To illustrate the dependence of the mobility function Φ_{V} on the concentration of surfactant in the continuous phase, in Fig. 12 we present theoretical curves, calculated in Ref. 138 for the nonionic surfactant Triton X-100, for the ionic surfactant SDS (+ 0.1 M NaCl) and for the protein bovine serum albumin (BSA). The parameter values, used to calculated the curves in Fig. 12, are listed in Table 4; Γ_∞ and K are parameters of the Langmuir adsorption isotherm used to describe the dependence of surfactant adsorption, surface tension, and Gibbs elasticity on the surfactant concentration (see Tables 1 and 2). As before, we have used the approximation $D_{1s} \approx D_1$ (surface diffusivity equal to the bulk diffusivity). The surfactant concentration in Fig. 12 is scaled with the reference concentration c_0, which is also given in Table 4; for Triton X-100 and SDS + 0.1 M NaCl, c_0 is chosen to coincide with the cmc. The driving force, F, was taken to be the buoyancy force for dodecane drops in water. The surface force F_s is identified with the van der Waals attraction; the Hamaker function $A_{\mathrm{H}}(h)$ was calculated by means of Eq. (86) (see below). The mean drop radius in Fig. 12 is $a = 20$ /μm. As seen in the figure, for such small drops $\Phi_{\mathrm{V}} \approx 1$ for Triton X-100 and BSA, i.e., the drop sur-

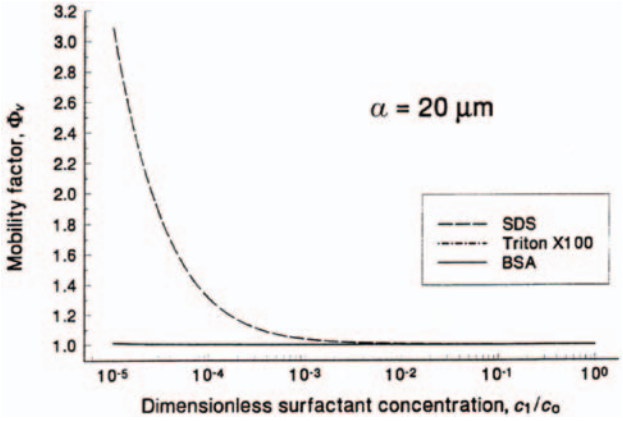

Figure 12 Theoretical dependence of the mobility factor Φ_V, on the surfactant concentration c_1, calculated in Ref. 138 for the nonionic surfactant Triton X-100, ionic surfactant SDS + 0.1 M NaCl, and the protein BSA; the curves for Triton X-100 and BSA coincide. The mean drop radius is $a = 20$ μm and the film thickness is $h \approx 10$ nm; the other parameters values are listed in Table 4.

faces turn out to be tangentially immobile in the whole concentration range investigated. On the other hand, Φ_V becomes considerably greater than unity for the lowest SDS concentrations, which indicates increased mobility of the drop surfaces.

3. Formation of Pimple

Let us consider two spherical emulsion drops approaching each other, which interact through the van der Waals attractive surface force. Sooner or later interfacial deformation will occur in the zone of drop-drop contact. The calculations (138) show that, if the drop radius a is greater than 80 μm, the drop interfaces bend inwards (under the action of the hydrodynamic pressure) and a *dimple* is formed in the contact zone; soon the dimple transforms into an almost plane-parallel film (Fig. 2D). In contrast, if the drop radius a is less than 80 μm, then at a given surface-to-surface distance $h = h_p$ the drop surface in the contact zone bends outwards and a *pimple* forms due to the van der Waals attraction (see the inset in Fig. 13). Correspondingly, h_p is called the pimpling distance. Since the size of the drops in an emulsion is usually markedly below 80 μm, we will consider here only the formation of a pimple.

The formation of pimples was discovered by Yanitsios and Davis (139) in computer calculations for emulsion drops from pure liquids, without any surfactant. Next, by means of numerical calculations, Cristini et al. (140) established the formation of a pimple for emulsion drops covered with insoluble surfactant in the case of negligible surface diffusion; their computations showed that rapid coalescence took place for $h < h_p$. A complete treatment of the problem for the formation of pimples was given in Ref. 138, where the effects of surface and bulk diffusion of surfactant, as well as the surface elasticity and viscosity, were taken into account, and analytical expressions were derived.

The origin of pimple formation is the fact that the van der Waals disjoining pressure, $\Pi \propto 1/h^3$, grows faster than the hydrodynamic pressure with decrease in h. For a certain distance, $h = h_p$, Π counterbalances the hydrodynamic pressure (138):

$$\frac{F - F_s}{\pi a h_p} \Phi_p (h_p; b, d, s_v) + \Pi(h_p) = 0 \qquad (59)$$

where Φ_p is the mobility factor for the pressure. Further, for a shorter distance between the drops, $h < h_p$, the pimples spontaneously grow until the drop surfaces touch each other and the drops coalesce. The pimple formation at $h = h_p$ can be interpreted as an onset of instability *without* fluctuations.

Analytical asymptotic expressions for the pressure mobility factor, Φ_p, can be found in Table 3. In general, Φ_p is to be calculated numerically. In the case of tangentially immobile surfaces of the drops Eq. (59) yields a very simple formula for the pimpling distance (138):

Table 4 Parameters for the Solutions of Triton X-100, SDS + 0.1 M NaCl, and BSA

	Triton X-100	SDS + 0.1 M NaCl	BSA
Γ_∞	1.75×10^{-6} mol/m^2	3.75×10^{-6} mol/m^2	0.38×10^{-6} mol/m^2
$1/K$	4.9×10^{-6} kg/m^3	1.4×10^{-3} kg/m^3	0.124×10^{-6} kg/m^3
D_1	2.6×10^{-10} m^2/s	6.0×10^{-10} m^2/s	1.0×10^{-10} m^2/s
c_0	0.4 kg/m^3 (cmc)	0.33 kg/m^3 (cmc)	0.6 kg/m^3
η_s	1.0×10^{-6} mPa.s	1.0×10^{-6} mPa.s	5.0×10^{-3} mPa.s

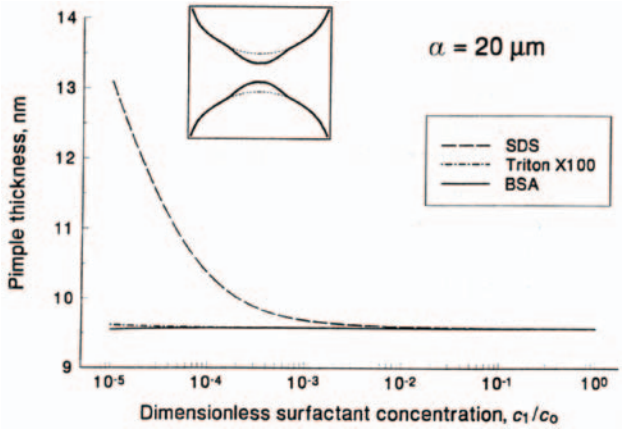

Figure 13 Calculated dependence of the pimple thickness, h_p, on the surfactant concentration, c_1, for emulsion films formed from aqueous solutions of SDS + 0.1 M NaCl, Triton X-100, and BSA; the parameters values used are listed in Table 4. The inset illustrates the shape of the drop surfaces in the zone of contact.

$$h_p = \sqrt{\frac{aA_H}{12F}} \qquad \text{(tangentially immobile surfaces)} \tag{60}$$

In the more complicated case of mobile drop surfaces Eq. (59) has to be solved numerically. Figure 13 shows calculated curves for the dependence of h_p versus the surfactant concentration; the parameter values used are the same as for Fig. 12 (see Table 4). Since the surfaces of the drops with BSA and Triton X-100 are tangentially immobile, the respective pimpling distance is practically constant (independent of surfactant concentration) and given by Eq. (60). The effect of surface mobility shows up for the emulsions with SDS + 0.1 M NaCl, for which the pimpling distance h_p is greater (Fig. 13). These calculations demonstrate that h_p is typically of the order of 10 nm.

If the pimpling distance is greater than the critical distance, $h_p > h_c$, then the pimpling will be the reason for coalescence. On the other hand, if $h_c > h_p$, then the coalescence will be caused by the fluctuation capillary waves (see the next subsection).

4. Transitional and Critical Distance

As already mentioned, when two emulsion drops approach each other, the attractive surface forces promote the growth of fluctuation capillary waves in the contact zone. At a given, sufficiently small surface-to-surface distance, called the transitional distance, h_t, the waves with a given length (usually the longest one) begin to grow; this is a transition from stability to instability. During the growth of the waves the gap width continues to decrease, which leads to destabilization and growth of waves with other lengths. Finally, the surfaces of the two drops touch each other owing to the enhanced interfacial undulations, and coalescence takes place. The latter act corresponds to a given mean surface-to-surface distance, called the critical thickness, h_c. The difference between the transitional and critical distance, $h_t > h_c$, is due to the fact that during the growth of the capillary waves the average film thickness continues to decrease, insofar as the drops are moving against each other driven by the force $F \text{—} F_s$. In the simpler case of immobile drops ($F \text{—} F_s = 0$), considered in Sec. III.C, one has $h_t = h_c$.

A general equation for determining h_t, which takes into account the effect of surface mobility, has been reported in Ref. 136:

$$[F - F_s]\Psi(\bar{d}) = \frac{\pi a^2 h_t^3}{32\sigma}\left[\left(\frac{\partial \Pi}{\partial h}\right)^2 - \frac{8\sigma}{a}\left(\frac{\partial^2 \Pi}{\partial h^2}\right)\right]_{h=h_t} \tag{61}$$

where

$$\bar{d} \equiv \frac{d}{h}, \qquad \Psi(\bar{d}) = \frac{(\bar{d}+2)\bar{d}^2}{4(\bar{d}+1)^2[(\bar{d}+1)\ln(\bar{d}+1) - \bar{d}]} \tag{62}$$

The function $\Psi(d)$ accounts for the effect of the surface mobility. For large interfacial elasticity one has $d \to 0$, see Eq. (53); then $\Psi \to 1$ and Eq. (61) acquires a simpler form, corresponding to drops of tangentially immobile interfaces. In the other limit, small interfacial elasticity, one has $d \gg 1$ and in such a case $\Psi \propto 1/\ln d$, i.e., Ψ decreases with the increase in d, that is, with the decrease in E_G. A numerical solution to this problem is reported in Ref. 24. The effect of the interfacial viscosity on the transitional distance, which is neglected in Eq. (61), is examined in Ref. 141. It is established therein that the critical distance, h_c, can be with in about 10% smaller than h_t.

The dependence of the transitional distance h_t on the surfactant concentration, calculated with the help of Eq. (61), is shown in Fig. 14; the three curves correspond to three fixed values of the mean drop radius a. The calculations are carried out for the system with SDS + 0.1 M NaCl in the aqueous phase (see Table 4); the oil phase is dodecane. One sees that the increase in surfactant concentration leads to a decrease in transitional thickness, which corresponds to a greater stability of the emulsion against coalescence. Physically this is related to the damping of the fluctuation cap-

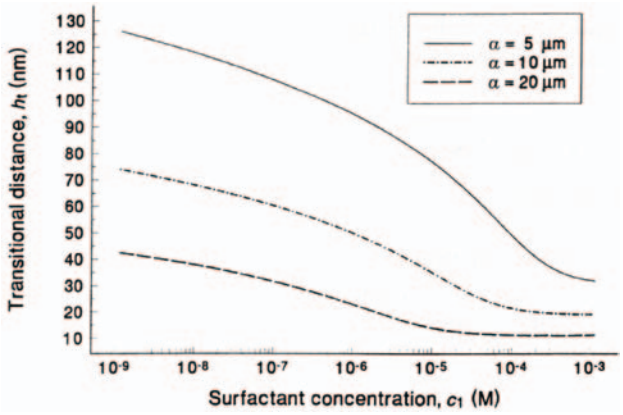

Figure 14 Dependence of the transitional distance between two drops, h_t, on the surfactant concentration, c_1, calculated with use of Eq. (61) for three values of the mean drop radius a.

illary waves by the adsorbed surfactant. Moreover, the transitional thickness for two approaching drops increases with the decrease in drop radius a (Fig. 14), which is exactly the opposite to the tendency for quiescent drops in Fig. 11 (we recall that $h_t = h_c$ for quiescent drops). The difference can be attributed to the strong dependence of the buoyancy force F on the drop radius a (such an effect is missing for the quiescent drops).

The comparison between Figs 13 and 14 shows that for the emulsion with SDS + 0.1 M NaCl one has $h_t > h_p$. In other words, the theory predicts that in this emulsion the drops will coalesce due to the fluctuation capillary waves, rather than owing to the pimpling.

If the coalescence is promoted by the van der Waals attractive surface force, from Eq. (61) one can deduce asymptotic expressions for h_t, corresponding to tangentially immobile drop surfaces ($\Psi = 1$) (136):

$$h_t = \left[a^2 A_{\mathrm{H}}^2/(128\pi\sigma F)\right]^{1/5}, \qquad \text{for} F \gg F_a \tag{63}$$

$$h_t = [5aA_{\mathrm{H}}/(12F)]^{1/2}, \qquad \text{for} F \ll \mathrm{F}_a \tag{64}$$

where $F_a = 12.66(a\sigma^2 A_H)^{1/3}$. In particular, if F is the buoyancy force, then $F \propto a^3$ and for small droplets ($F \ll F_a$) one obtains $h_t \propto 1/a$, i.e., the critical thickness markedly increases with the decrease in droplet radius.

B. Interaction Between Deforming Emulsion Drops

1. Drops of Tangentially Immobile Surfaces

In this subsection we consider the case in which a liquid film is formed in the zone of contact between two emulsion drops (see Fig. 7). Such a configuration appears between drops in floes and in concentrated emulsions, including creams.

In a first approximation, one can assume that the viscous dissipation of kinetic energy happens mostly in the thin liquid film intervening between two drops. (In reality, some energy dissipation happens also in the transition zone between the film and the bulk continuous phase.) If the drop interfaces are tangentially immobile (owing to adsorbed surfactant), then the velocity of approach of the two drops can be estimated by meanss of the Reynolds formula for the velocity of approach of two parallel solid disks of radius R, equal to the film radius (142):

$$V_{\mathrm{Re}} = \frac{2h^3 F_{\mathrm{tot}}}{3\pi\eta_{out} R^4} \tag{65}$$

As usual, here h is the film thickness, and F_{tot} is the total force exerted on a drop (2):

$$F_{\mathrm{tot}} = F - F_s - F_{\mathrm{def}} \tag{66}$$

As before, F is the applied external force (buoyancy, centrifugal force, Brownian force, etc.); F_s is the surface force of intermolecular origin, which for deformable drops can be expressed in the form (2, 143):

$$F_s = -\frac{dW}{dh}, \qquad W(R,h) \approx \pi R^2 f(h) + \pi a \int_h^\infty f(\hat{h})d\hat{h} \tag{67}$$

where

$$f(h) \equiv \int_h^\infty \Pi(\hat{h})d\hat{h} \tag{68}$$

is the interaction free energy per unit area of a plane-parallel liquid film, and W is the drop - drop interaction energy due to surface forces, which is a sum of contributions from the planar film and the transition zone film - bulk liquid; for $R = 0$, Eq. (67) reduces to Eq. (48). Finally, F_{def} is a force originating from the deformation of the drop interfaces (2):

$$F_{\mathrm{def}} = -\frac{d(W_{\mathrm{dil}} + W_{\mathrm{bend}})}{dh} \tag{69}$$

where W_{dil} is the work of interfacial dilatation (143—145),

$$W_{dil} = \sigma \frac{\pi R^4}{2a^2} + \frac{1}{2} E_G \left[\frac{\pi R^4}{2a^2} \right]^2 + \cdots, \text{ for } \left[\frac{R}{a} \right] \ll 1 \tag{70}$$

and W_{bend} is the work of interfacial bending (146):

$$W_{bend} = -2\pi R^2 B_0 / a, \quad (R/a)^2 \ll 1 \tag{71}$$

where $B_0 = -4k_c H_0$ is the interfacial bending moment; H_0 is the so-called spontaneous curvature, and k_c is the interfacial curvature elastic modulus.

Initially, the two approaching drops are spherical. The deformation in the zone of contact begins when the surface-to-surface distance reaches a certain threshold value, called the inversion thickness, h_{inv}. One can estimate the inversion thickness from the simple expression $h_{inv} = F/(2\pi\sigma)$ (see, e.g., Refs 98 and 121). The generalized form of the latter equation, accounting for the contribution of the surface forces, reads (136):

$$h_{inv} = \frac{F}{2\pi\sigma} + \frac{a}{2\sigma}[h_{inv}\Pi(h_{inv}) - f(h_{inv})] \tag{72}$$

The inversion thickness can be determined by solving Eq. (72) numerically.

A generalized expression for the velocity $V = -dh/dt$, which takes into account the energy dissipation in both film and the transition zone film - bulk liquid, has been derived in Refs 2 and 147:

$$\frac{1}{V} = \frac{1}{V_{Re}} + \frac{1}{V_{Ta}} + \frac{1}{\sqrt{V_{Re} V_{Ta}}} \tag{73}$$

where the Taylor velocity, V_{Ta}, and the Reynolds velocity, V_{Re}, are defined by means of Eqs (47) and (65). For R→0 (nondeformed spherical drops), Eq. (73) reduces to $V = V_{Ta}$. On the other hand, for $h \to 0$ one has $1/V_{Ta} \ll 1/V_{Re}$, and then Eq. (73) yields $V \to V_{Re}$. Substituting Eqs (47) and (65), and assuming $F \gg (F_s + F_{def})$ one can bring Eq. (73) into the form (147):

$$\frac{V_{Ta}}{V} = 1 + \frac{R^2}{ha} + \frac{R^4}{h^2 a^2} \tag{74}$$

One sees that $V \to V_{Ta}$ for $R^2/(ha) \ll 1$. If the external force F is predominant, then $R^2 \approx aF/(2\pi\sigma)$, $h_{inv} \approx F/(2\pi\sigma)$ and it follows that $R^2/a \approx h_{inv}$ (97, 135); the substitution of the latter equation into Eq. (74) yields:

$$\frac{V_{Ta}}{V} \approx 1 + \frac{h_{inv}}{h} + \frac{h_{inv}^2}{h^2} \tag{75}$$

Equation (75) shows that for $h \le h_{inv}$ the velocity V becomes considerably smaller than V_{Ta}.

2. Effect of Surface Mobility

When the surfactant is soluble only in the *continuous* phase (we will call such a system "System I", see Fig. 15), turns out that the respective rate of film thinning V_1 is affected by the surface mobility mainly through the Gibbs elasticity E_G, just as it is for foam films (97, 121):

$$\frac{V_1}{V_{Re}} \approx 1 + \frac{1}{\varepsilon_f}, \qquad \frac{1}{\varepsilon_f} = \frac{6\eta_1 D_{1s}}{hE_G} + \frac{3\eta_1 D_1}{\Gamma_1} \left[\frac{\partial c_1}{\partial \sigma} \right]^{(e)} \tag{76}$$

Here, ε_f is the so called *foam parameter*, and η_1 is the viscosity in the surfactant-containing phase (Liquid 1 in Fig. 15); the influence of the transition zone film - bulk liquid is not accounted for in Eq. (76). Note that the bulk and surface diffusion fluxes (see the terms with D_{1s} and D_1 in the latter equation), which tend to damp the surface tension gradients and to restore the uniformity of the adsorption monolayers, accelerate the film thinning (Fig. 1). Moreover, since D_{1s} in Eq. (76) is divided by the film thickness h, the effect of surface diffusion dominates that of bulk diffusion for small values of the film thickness. On the other hand, the Gibbs elasticity E_G (the Marangoni effect) decelerates the thinning. Equation (76) predicts that the rate of

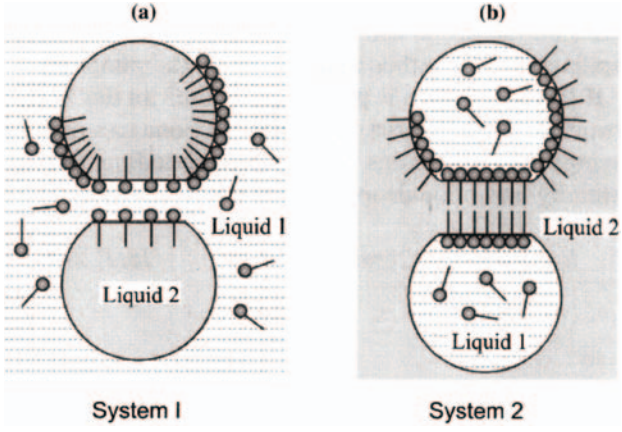

Figure 15 Two complementary types of emulsion system obtained by a mere exchange of the continuous phase with the disperse phase. The surfactant is assumed to be soluble only in Liquid 1. (a) Liquid 2 is the disperse phase; (b) Liquid 2 is the continuous phase.

thinning is not affected by the circulation of liquid in the droplets, i.e., System I really behaves as a foam system.

It was established theoretically (97, 133) that when the surfactant is dissolved in the *drop* phase (System II in Fig. 15) it remains uniformly distributed throughout the drop surface during film thinning, and interfacial tension gradients do not appear. This is the result of a powerful supply of surfactant, which is driven by convective diffusion from the bulk of the drops toward their surfaces. For that reason, the drainage of the film surfaces is not opposed by surface-tension gradients, and the rate of film thinning, V_{II}, is the same as in the case of pure liquid phases (97, 133):

$$\frac{V_{II}}{V_{Re}} \approx \frac{1}{\varepsilon_e} \approx \frac{\eta_1 \delta}{\eta_2 h} \approx \left[\frac{108\pi\eta_1^3 R^4}{\rho_2 \eta_2 h^4 F}\right]^{1/3} \tag{77}$$

Here, η_e is called the emulsion parameter, δ is the thickness of the hydrodynamic boundary layer inside the drops, and ρ_2 and η_2 are the mass density and dynamic viscosity of Liquid 2, which does not contain dissolved surfactant. The validity of Eq. (77) was confirmed experimentally (134).

The only difference between the two systems in Fig. 15 is the exchange of the continuous and drop phases. Assume for simplicity that V_{Re} is the same for both systems. In addition, usually $\varepsilon_f \approx 0.1$ and $\varepsilon_e \approx 10^{-2}$ to 10^{-3}. From Eqs (76) and (77) one then obtains (97, 121, 133):

$$\frac{V_{II}}{V_I} \approx \frac{\varepsilon_f}{\varepsilon_e} \approx \frac{0.1}{10^{-2}\ \text{to}\ 10^{-3}} \approx 10\ \text{to}\ 100 \quad \text{(deformed drops)} \tag{78}$$

Hence, the rate of film thinning in System II is much greater than that in System I. Therefore, the location of the surfactant has a dramatic effect on the thinning rate and, thereby, on the drop lifetime. Note also that the interfacial tension in both systems is the same. Hence, the mere phase inversion of an emulsion, from Liquid 1-in-Liquid 2 to Liquid 2-in-Liquid 1 (Fig. 15), could change the emulsion lifetime by orders of magnitude. As discussed in Sec. V, the situation with interaction in the Taylor regime (between spherical, nondeformed drops) is similar. These facts are closely related to the explanation of the Bancroft rule for the stability of emulsions (see Sec. V) and the process of chemical demulsification (1).

Equations (76) and (77) do not take into account the hydrodynamic interactions across the transition zone around the film, which can be essential if the film radius R is relatively small. In the latter case the effect of surface viscosity becomes important for System I. Equation (76) can then be presented in a more general form (137).

$$\frac{V_I}{V_{Re}} = \Phi_v(h; b, d, R, s_v) \tag{79}$$

where Ω_V is a mobility function. In Ref. 137 a general, but voluminous, analytical expression for Ω_V is derived in the form of an infinite series expansion; it accounts for the effects of surface elasticity, surface viscosity, and bulk and surface diffusion. In some special cases this infinite series can be summed up and closed expressions for Ω_V can be obtained. Such is the case when the effect of the surface viscosity is negligible, $S_V \to 0$; the respective expression for Ω_V reads (137):

$$\frac{1}{\Phi_v} = \frac{1}{1+b+h_s/h} + \frac{2h}{N_R^4 h_s}\left\{\left[\frac{h}{h_s}(1+b)(1-N_R^2)+1\right]\ln\left[1+\frac{h_s}{h(1+b)}\right] + N_R^2 - 1\right\} \tag{80}$$

where the dimensionless parameter $N_R = R/(ah)^{1/2}$ accounts for the effect of the film radius. In the case of emulsion drops $N_R \equiv$ however, if experiments with emulsion films are performed in the experimental cell of Scheludko and Exerowa (148, 149), which allows independent control of R, then one usually has $N_R \gg 1$. (The original experiments in Refs 148 and 149 have been carried out with foam films, but a similar technique can be appllied to investigate emulsion films, see, e.g., Refs 91 and 150—158.) In the limit of large plane-parallel film, $N_R \gg 1$, Eq. (80) reduces to the result of Radoev *et al*. (159): $V_1/V_{Re} = 1 + b + h_s/h$ (effect of the transition zone negligible). For insoluble surfactants the parameter b in Eq. (80) must be set equal to zero.

Under certain experimental conditions, like those in Ref. 60, the motion of surfactant along an oil-water interface represents a flow of a two-dimensional *incompressible viscous* fluid. In such a case Eq. (79) acquires the following specific form (137):

$$\frac{1}{V_I} = \frac{1}{V_{Ta}} + \frac{1}{V_{Re}} + \frac{1}{\sqrt{V_{Ta}V_{Re}}} - \frac{1}{2s_v}\left[\frac{1}{V_{Ta}} + \frac{1}{V_{Re}} + \frac{1}{\sqrt{V_{Ta}V_{Re}}} + \frac{N_R^2}{3\sqrt{V_{Ta}V_{Re}}}\right] \tag{81}$$

Equation (81) is a truncated power expansion for $S_v \gg 1$. In the limit of tangentially immobile interfaces ($S_v \to \infty$) Eq. (81) reduces to Eq. (73).

To illustrate the effects of various factors on the velocity of approach of two deforming emulsion drops (Fig. 15a) we used the general expression from Ref. 137 (the infinite series expansion) to calculate the mobility factor Ω_v; the results are shown in Figs 16 and 17. First of all, in Fig. 16 we illustrate the effects of bulk and surface diffusion. For that reason $\Omega_v \equiv V_1/V_{Re}$ is plotted versus the parameter b, related to the bulk diffusivity, for various values of h_s/h; h_s is related to the surface diffusivity, see Eq. (54). If the hydrodynamic interaction were operative only in the film, then one would obtain $V_1/V_{Re} \geq 1$. However, all calculated values of V_1/V_{Re} are less than 0.51 (Fig. 16); this fact is evidence for a significant effect of the hydrodynamic interactions in the transition zone around the film. Moreover, in Fig. 16 one sees that for $b > 10$ the mobility factor Ω_v is independent of the surface diffusivity. On the other hand, for $b < 10$ a considerable effect of surface diffusivity shows up: the greater the surface diffusivity effect, h_s/h, the greater the interfacial mobility factor Ω_v. For the upper curve in Fig. 16 the interfacial mobility is determined mostly by the effect of surface viscosity, S_v, which is set equal to unity for all curves in the figure.

To illustrate the effect of surface viscosity, S_v, in Fig. 17 we have plotted the mobility factor $\Omega_v = V_1/V_{Re}$ versus b for three different values of S_v. For the higher surface viscosities, $S_v = 1$ and 5, and the mobility factor is $V_1/V_{Re} < 1$, which again indicates a strong hydrodynamic interaction in the transition zone around the film. For the lowest surface viscosity, $S_v = 0.1$, the mobility factor is sensitive to the effect of bulk diffusion, characterized by b: for $b > 3$ we have $V_1/V_{Re} > 1$, i.e., we observe a considerable rise in the interfacial mobility (Fig. 17).

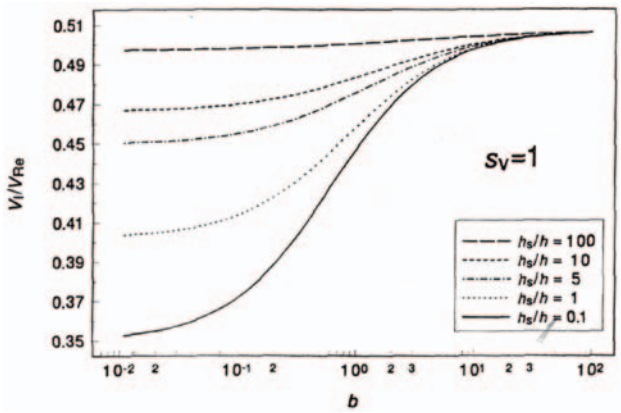

Figure 16 Effect of the surface diffusion parameter, h_s/h, on the variation of the mobility factor, $\Omega_v = V_1/V_{Re}$, with the bulk diffusion parameter, b, for fixed S_v and $N_R = 1$.

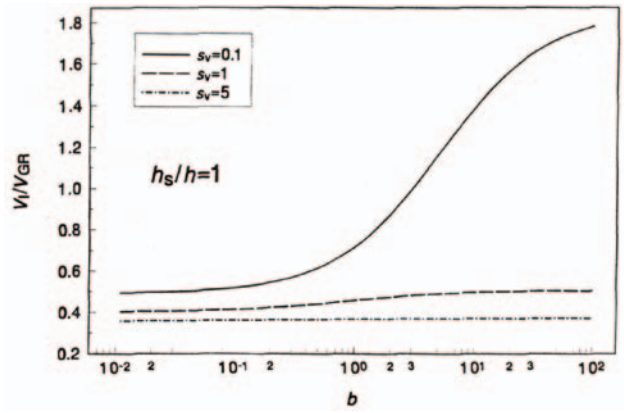

Figure 17 Effect of the surface viscosity parameter, S_v, on the variation of the mobility factor, $\Omega_v = V_1/V_{Re}$, with the bulk diffusion parameter, b, for fixed $h_s/h = 1$ and $N_R = 1$.

3. Critical Thickness of the Film Between Two Deforming Drops

As already mentioned, the transition from stability to instability occurs when the thickness of the gap between two colliding emulsion drops decreases down to a "transitional" thickness h_t. For $h_t > h > h_c$ the film continues to thin, while the instabilities grow, until the film ruptures at the critical thickness $h = h_c$.

Equation (61) determines the transitional distance between two spherical emulsion drops. An analog of this equation for the case of two deformed drops (Fig. 15a) has been obtained in the form of a transcendental equation (2, 136):

$$\frac{2h_t + d}{h_t + d} = \frac{h_t R^2 [\Pi'(h_t)]^2}{8\sigma[2\sigma/a - \Pi(h_t)]}, \qquad \Pi' \equiv \frac{\partial \Pi}{\partial h} \tag{82}$$

Equation (82) shows that the disjoining pressure significantly influences the transitional thickness h_t. The effect of surface mobility is characterized by the parameter d, see Eq. (53); in particular, $d = 0$ for tangentially immobile interfaces. Equation (82) is valid for $\prod < 2\sigma/a$, i.e., when the film thins and ruptures before reaching its equilibrium thickness, corresponding to $\prod = 2\sigma/a$ [cf. Eqs (42), (43), and (59)].

The calculation of the transitional thickness h_t is a prerequisite for computing the critical thickness h_c, which can be obtained as a solution to the equation (95, 96):

$$h_c^2 = \frac{2kT}{I(h_c, h_t)} \exp\left[\frac{I(h_c, h_t)}{4\sigma}\right] \tag{83}$$

where $I(h_t,h_c)$ represents the following function:

$$I(h_c, h_t) = \Pi'(h_t)R^2 \int_{h_c}^{h_t} \frac{\Pi' dh}{\Phi_v(h)[2\sigma/a - \Pi(h)]} \tag{84}$$

In the special case of tangentially immobile interfaces and large film (negligible effect of the transition zone) one has $\Omega_V(h) = 1$, and the integration in Eq. (84) can be carried out (95):

$$I(h_c, h_t) = \Pi'(h_t)R^2 \ln\left[\frac{2\sigma/a - \Pi(h_c)}{2\sigma/a - \Pi(h_t)}\right] \tag{85}$$

Note that Eqs (82)-(85) hold not only for an emulsion film formed between two oil drops, but also for a foam film intervening between two gas bubbles. In Fig. 18 we compare the prediction of Eqs (82)-(84) with experimental data for h_c versus R, obtained by Manev et al. (120) for foam films formed from an aqueous solution of 0.43 mM SDS + 0.1 M NaCl. The mobility factor $\Omega_V(h)$ was calculated by using the exact expression (the infinite series) from Ref. 137. Parameters such as ω, E_G, Γ_1 and $\partial\Gamma_1/\partial c_1$, see Eqs (53)-(55), are obtained from the experimental fit in Ref. 17, in the same way as the numerical data in Fig. 5 have been obtained (see Sec. II.A.2). The disjoining pressure was attributed to the van der Waals attraction: $\Pi = -A_H/(6\pi h^3)$. To account for the effect of the electromagnetic retardation on the dispersion

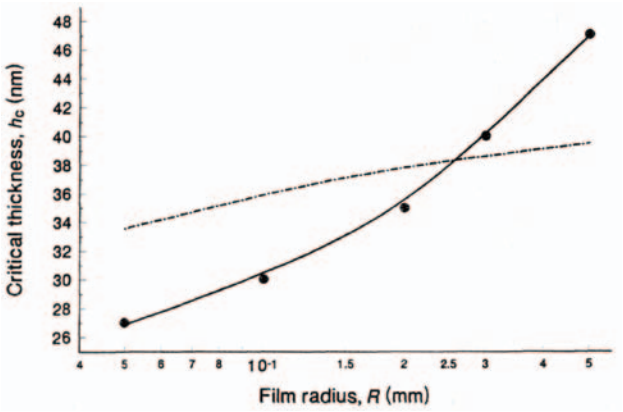

Figure 18 Critical thickness, h_c, vs radius, R, of a foam film formed from aqueous solution of 0.43 mM SDS + 0.1 M NaCl: comparison between experimental points, measured by Manev et al. (120), with our theoretical model based on Eqs. (82)-(87) (the solid line) and the model by Malhotra and Wasan (116) (the dashed line).

interaction, we used an expression proposed by Russel et al. (160):

$$A_H(h) = \frac{3h_P\nu}{4\pi} \frac{(n_0^2 - n_w^2)^2}{(n_0^2 + n_w^2)^{3/2}} \int_0^\infty \frac{(1 + 2\tilde{h}z)\exp(-2\tilde{h}z)}{(1 + 2z^2)^2} dz \tag{86}$$

Here, $h_P = 6.63 \times 10^{-34}$ J.s is the Planck constant, $\nu \approx 3.0 \times 10^{15}$ Hz is the main electronic absorption frequency, and n_0 and n_w are the refractive indices of the nonaqueous and aqueous phases; for a foam film $n_0 = 1$ and $n_w = 1.333$. The dimensionless thickness h is defined by the expression:

$$\tilde{h} = n_w(n_0^2 + n_w^2)^{1/2} \frac{2\pi\nu h}{c} \tag{87}$$

where $c = 3.0 \times 10^{10}$ cm/s is the speed of light. For small thickness A_H, as given by Eqs (86) and (87), is constant, whereas for large thickness h one obtains $A_H \propto h^{-1}$. The solid line in Fig. 18 was calculated with the help of Eqs (82)-(87) *without* using any adjustable parameters; one sees that there is an excellent agreement between this theoretical model and the experiment.

The dot-dashed line in Fig. 18 shows the prediction of the theoretical model by Malhotra and Wasan (116). Our calculations showed that for the specific surfactant and salt concentrations (0.43 mM SDS + 0.1 M NaCl) the interfaces are almost tangentially immobile. Moreover, in these experiments the film radius R is sufficiently large, which allows one to neglect effects of the transition zone, i.e., to ignore the last two terms in Eq. (73). Consequently, the difference between the model from Ref. 116 and the experimental data (Fig. 18) cannot be attributed to the latter two effects (interfacial mobility and transition zone), which have not been taken into account in Ref. 116. The main reasons for the difference between the output of Ref. 116 and the experiment are that (1) these authors have, in fact, calculated h_t, and identified it with h_c; and (2) a constant value of A_H has been used, instead of Eq. (86), i.e., the electromagnetic retardation effect has been neglected. It is interesting to note that the retardation effect turns out to be important in the experimental range of critical thicknesses, in this specific case: 25 nm < h_c < 50 nm.

V. INTERPRETATION OF THE BANCROFT RULE

A simple rule connecting the emulsion stability with the surfactant properties was formulated by Bancroft (161).

The Bancroft rule states that "in order to have a stable emulsion the surfactant must be soluble in the continuous phase." Most of the emulsion systems obey this rule, but some exclusions have also been found (162). The results on drop-drop interactions, presented in Sec. IV, allow one to give a semiquantitative interpretation of the rule and the exclusions (1, 2, 163).

According to Davies and Rideal (6), both types of emulsions (water-in-oil and oil-in-water) are formed during the homogenization process, but only the one with lower coalescence rate survives. If the initial drop concentration for the two emulsions (Systems I and II, see Fig. 15) is the same, the corresponding coalescence rates for the two emulsions will be (approximately) proportional to the respective velocities of film thinning, V_I and V_{II} (163):

$$\frac{\text{Rate I}}{\text{Rate II}} \approx \frac{V_I}{V_{II}} \tag{88}$$

A. Case of Deforming Drops

In the case of *deforming* drops, using Eqs (65), (76), and (77), one can represent Eq. (88) in the form (1, 163):

$$\frac{\text{Rate I}}{\text{Rate II}} \approx (486\rho_2 D_{1s}^3)^{1/3} \left[\frac{h_{c,I}^3}{h_{c,II}^2}\right]^{1/3} \left[\frac{\eta_2}{R^2}\right]^{1/3} \frac{2\sigma/a - \Pi_I}{E_G(2\sigma/a - \Pi_{II})^{2/3}} \tag{89}$$

where $h_{c,I}$ and $h_{c,II}$ denote the critical thickness of film rupture for the two emulsion systems in Fig. 15; Π_I and Π_{II} denote the disjoining pressure of the respective films. To obtain Eq. (89) we have also used the estimate $F_{tot} \approx \pi(2\sigma/a - \Pi)R^2$ (see Ref. 149). The product of the first three multipliers on the right-hand side of Eq. (89), which are related to the *hydrodynamic* stability, is 8×10^{-5} dyn$^{2/3}$cin$^{-1/3}$ for typical parameter values (1). The last multiplier in Eq. (89) accounts for the *thermodynamic* stability of the two types of emulsion film. Many conclusions regarding the type of emulsion formed can be drawn from Eq. (89) (1, 62, 163).

In thick films the disjoining pressures, Π_I and Π_{II}, are zero, and then the ratio in Eq. (89) will be very small. Consequently, emulsion I (surfactant soluble in the continuous phase) will coalesce much more slowly than emulsion II; hence, emulsion I will survive. Thus, we obtain an explanation of the empirical Bancroft rule. The emulsion behavior in this case is controlled mostly by the hydrodynamic factors, i.e., the factors related to the *kinetic* stability.

The disjoining pressure, Π, can substantially change, and even reverse, the behavior of the system if it is comparable by magnitude with the capillary pressure, $2\sigma/a$. For example, if $(2\sigma/a - \Pi_{II}) \to 0$ at a finite value of $2\sigma/a - \Pi_I$, then the ratio in Eq. (89) may become much larger than unity, which means that System II will become *thermodynamically* stable. This fact can explain some exclusions from the Bancroft rule, like that established by Binks (162). Moreover, a large stabilizing disjoining pressure is operative in emulsions with a high volume fraction of the disperse phase, above 95% in some cases (164).

The Gibbs elasticity, E_G, favors the formation of emulsion I (Fig. 15a), because it slows down the film thinning. On the other hand, increased surface diffusivity, $D_{1,S}$, decreases this effect, because it helps the interfacial-tension gradients to relax, thus facilitating the formation of emulsion II.

The film radius, R, increases, whereas the capillary pressure, $2\sigma/a$, decreases with the rise in drop radius, a. Therefore, larger drops will tend to form emulsion I, although the effect is not very pronounced, see Eq. (89). The difference between the critical thicknesses of the two emulsions affects only slightly the rate ratio in Eq. (89), although the value of h_c itself is important.

The viscosity of the surfactant-containing phase, η_1, does not appear in Eq. (89); there is only a weak dependence on η_2. This fact is consistent with the experimental findings about a negligible effect of viscosity (see Ref. 6, p. 381 therein).

The interfacial tension, σ, affects directly the rate ratio in Eq. (89) through the capillary pressure, $2\sigma/a$. The addition of electrolyte would affect mostly the electrostatic component of the disjoining pressure (see Fig. 8a), which is suppressed by the electrolyte; the latter has a destabilizing effect on O/W emulsions. In the case of ionic surfactant solutions the addition of electrolyte rises the surfactant adsorption and the Gibbs elasticity (see Fig. 5), which favors the stability of emulsion I.

Surface-active additives (such as cosurfactants, demulsifiers, etc.) may affect the emulsifier partitioning between the phases and its adsorption, thereby changing the Gibbs elasticity and the interfacial tension. The surface-active additive may change also the surface charge (mainly through increasing the spacing among the emulsifier ionic headgroups), thus decreasing the electrostatic disjoining pressure and favoring the W/O emulsion. Polymeric surfactants and adsorbed proteins increase the steric repulsion between the film surfaces; they may favor either of the emulsions O/W or W/O, depending on their conformation at the in-

terface and their surface activity.

The temperature affects strongly both the solubility and the surface activity of nonionic surfactants (165). It is well known that at higher temperatures nonionic surfactants become more oil soluble, which favors the W/O emulsion. These effects may change the type of emulsion formed at the phase-inversion temperature (166). The temperature effect has numerous implications, two of them being the change in the Gibbs elasticity, E_G, and the interfacial tension, σ.

B. Case of Spherical Drops

Equation (89) was obtained for deforming emulsion drops, i.e., for drops which can approach each other at a surface-to-surface distance less than the inversion thickness h_{inv}, see Eq. (72). Another possibility is the drops to remain *spherical* during their collision, up to their eventual coalescence at $h = h_c$; in such a case the expressions for V_I and V_{II}, which are to be substituted in Eq. (88), differ from Eqs (76) and (77).

Let us first consider the case of System II (surfactant inside the drops, Fig. 15b) in which case the two drops approach each other like drops from pure liquid phases (if only the surface viscosity effect is negligible). Therefore, to estimate the velocity of approach of such two aqueous droplets one can use the following approximate expression, which directly follows from Eq. (49) for $\xi \gg 1$:

$$V_{II}/V_{Ta}^{(II)} \approx 0.811 \frac{\eta_2}{\eta_1}\sqrt{\frac{a}{h}} \tag{90}$$

(For the system from Fig. 15b one is to set $\eta_{out} = \eta_2$ and $\eta_{in} = \eta_1$.) On the other hand, the velocity V_1 of droplet approach in System I can be expressed by means of Eq. (52). Note that the Taylor velocities for Systems I and II, $V^{(I)}{}_{Ta}$ and $V^{(II)}{}_{Ta}$, are different because of differences in viscosity and droplet-droplet interaction, see Eq. (47). By combining Eqs (47), (52), (88), and (90) we then arrive at the following criterion for formation of emulsions of type I or II (2):

$$\frac{\text{Rate I}}{\text{Rate II}} \approx 1.233 \frac{h_s}{2h}\sqrt{\frac{h}{a}}\left[\frac{\bar{d}+1}{\bar{d}}\ln(\bar{d}+1)-1\right]^{-1}\frac{(F-F_s)_I}{(F-F_s)_{II}} \tag{91}$$

where $\bar{d} \equiv d/h$; see Eqs (53)-(55) for the definitions of d, b, and h_s. In the case of large surface (Gibbs) elasticity, $E_G \gg 1$, one has $' \ll 1$; hence, one can expand the logarithm in Eq. (91) to obtain (2):

$$\frac{\text{Rate I}}{\text{Rate II}} \approx 1.233\sqrt{\frac{h_c}{a}}\frac{1+b}{1-\bar{d}/3+O(\bar{d}^2)}\frac{(F-F_s)_I}{(F-F_s)_{II}} \tag{92}$$

Here, we have substituted h_c for h, which is fulfilled at the moment of coalescence. For typical emulsion systems one has $a \gg h_c$, and then Eq.(92) yields Rate I/Rate II $\ll 1$; therefore, System I (with surfactant in the continuous phase, Fig. 15a) will survive. This prediction of Eq. (92) for spherical drops is analogous to the conclusion from Eq. (89) for deformable drops. Both these predictions essentially coincide with the Bancroft rule and are valid for cases in which the *hydrodynamic* stability factors prevail over the *thermodynamic* ones. The latter become significant close to the equilibrium state, $F_s \approx F$, and could bring about exclusions from the Bancroft rule, especially when $(F - F_s)_{II} \to 0$. The following conclusions, more specific for the case of *spherical* drops, can be also drawn from Eqs. (91) and (92).

For larger droplets (larger a) the transitional distance h_t (and the critical distance h_c as well) is smaller (see Fig. 14). It then follows from Eq. (91) that the difference between the coalescence rates in Systems I and II will become larger (2). On the contrary, the difference between Rates I and II decreases with the reduction in droplet size a, which is accompanied by an increase in the critical thickness h_c. Note that this effect of a cannot be derived from the criterion for deforming drops, Eq. (89).

The effect of the bulk viscosity is not explicitly present in Eq. (92), although there could be some weak implicit dependence through the parameters d and b [see Eqs (53) and (55)]. This conclusion agrees with the experimental observations about a very weak dependence of the volume fraction of phase inversion on the viscosity of the continuous phase (6).

The increase in bulk and surface diffusivities, D_1 and D_{1s}, which tend to damp the surface-tension gradients, leads to an increase in the parameters b and d, which decreases the difference between Rates I and II [see Eqs (53), (55), and (92)]. In contrast, the increase in the Gibbs elasticity, E_G, leads to a decrease in d and thus favors the survival of System I. These are the same tendencies as for deforming drops (Sec. V. A). In the limit of tangentially *im-*

mobile interfaces ($E_G \to \infty$) one has $d = 0$ and $b = 0$ and the criterion, Eq. (92), further simplifies (2):

$$\frac{\text{Rate I}}{\text{Rate II}} \approx \frac{V_{\text{I}}}{V_{\text{II}}} \approx 1.233\sqrt{\frac{h_c}{a}}\frac{(F-F_s)_{\text{I}}}{(F-F)_{\text{II}}} \qquad (E_G \to \infty) \tag{93}$$

The effect of surface viscosity, η_S, is neglected when deriving Eqs (91)-(93). Based on the hydrodynamic equations one can estimate that this effect is really negligible when (2)

$$\frac{\eta a^2}{\eta_s h} \gg 1 \tag{94}$$

where η represents the bulk viscosity, which is assumed to be of the same order of magnitude for the liquids inside and outside the drops. If for a certain system, or under certain conditions, the criterion, Eq. (94), is not satisfied, one can expect that the surface viscosity will suppress the interfacial mobility for both Systems I and II. The difference between Rates I and II will be then determined mostly by thermodynamic factors, such as the surface force F_S.

Although Eqs (89) and (91) lead us to some more general conclusions than the original Bancroft rule (e.g., the possibility for inversion of the emulsion stability owing to disjoining pressure effects), we neither claim that the Bancroft rule, or its extension based on Eqs. (89) and (91), have general validity, nor that we have given a general explanation of the emulsion stability. The coagulation in emulsions is such a complex phenomenon, influenced by too many different factors, that according to us any attempt at formulating a *general* explanation (or criterion) is hopeless. Our treatment is theoretical and as every theory, it has limitations inherent to the model used and therefore is valid only under specific conditions. It should not be applied to a system where these conditions are not fulfilled. The main assumptions and limitations of the model are (2): the fluctuation-wave mechanism for coalescence is assumed to be operative (see Fig. 10); the surfactant transfer on to the surface is under diffusion or electro-diffusion control; parameter b defined by Eq. (55) does not account for the demicellization kinetics for $c_1 >$ cmc; and the effect of surface viscosity is not taken into account in Eqs (89) and (91). Only *small* perturbations in the surfactant distribution, which are due to the flow, have been considered; however, under strongly nonequilibrium conditions (like turbulent flows) we could find that new effects come into play, which may significantly alter the trend of the phenomenon.

VI. KINETICS OF COAGULATION IN EMULSIONS

A. Types of Coagulation in Emulsions

The coagulation in an emulsion is a process in which the separate emulsion drops merge to form larger drops (coalescence) and/or assemble into flocs (flocculation), see Fig. 2. If the films intervening between the drops in a floc are unstable, their breakage is equivalent to coalescence, see step D→C in Fig. 2. In other words, the coagulation in an emulsion includes flocculation and coalescence, which could occur as parallel or consecutive processes.

Various *experimental methods* for monitoring the kinetics of coagulation in emulsions have been developed, such as the electroacoustic method (167), direct video-enhanced microscopic investigation (168), and ultrasonic attenuation spectroscopy (169).

To a great extent the occurrence of coagulation is determined by the energy, $W(R, h)$, of the interaction between two drops. Equation (67), which defines $W(R, h)$, can be applied to any type of surface force (irrespective of its physical origin) if only the range of action of this force is much smaller than the drop radius a. In Ref. 2 one can find theoretical expressions for the components of W stemming from various surface forces: electrostatic, van der Waals, ionic, correlations, hydration repulsion, protrusion and steric interactions, oscillatory structural forces, etc.

If the two drops remain spherical during their interaction (i.e., there is no film in the contact zone and consequently $R = 0$), then W depends only on a single parameter, $W = W(h)$; as usual, h is the surface-to-surface distance between the two drops. When the approach of the two drops is accompanied by the formation and expansion of a film in the contact zone (Fig. 7), then one can characterize the interaction by $W(h)$, which is obtained by averaging $W(R, h)$ over all configurations with various R at fixed h (see Ref. 143).

The shape of $W(h)$, or $\Pi(h)$, qualitatively resembles that of $\eta(h)$ (see Fig. 6). In particular, if only electrostatic and van der Waals interactions are operative, the shape of the dependence $W = W(h)$ resembles Fig. 6a, where an electrostatic barrier is present. The coagulation is called *fast* or *slow*, depending on whether that electrostatic barrier is less than kT or higher than kT. In addition, the flocculation is termed *reversible* or *irreversible*, depending on whether the depth of the primary minimum (that on the left from the barrier in Fig. 6a) is comparable with kT or much greater than kT. The driving forces of coagulation can be the fol-

lowing:

1. The *body forces*, such as gravity and centrifugation, cause rising or sedimentation of the droplets, depending on whether their mass density is smaller or greater than that of the continuous phase. Since drops of different size move with different velocities, they are subjected to frequent collisions, leading to drop aggregation or coalescence, called *orthokinetic coagulation*.
2. The *Brownian stochastic force* dominates the gravitational body force for droplets, which are smaller than 1 μm. Thus, the Brownian collision of two droplets becomes a prerequisite for their flocculation and/or coalescence, which is termed *perikinetic coagulation*.
3. The heating of an emulsion produces *temperature gradients*, which in their own turn cause thermocapillary migration of the droplets driven by thermally excited gradients of surface tension (170—172):

$$\nabla_s \sigma = -\frac{E_T}{T}\nabla_s T \qquad E_T \equiv -\left(\frac{\partial \sigma}{\partial \ln T}\right)_{\Gamma_1} \tag{95}$$

Here, ∇_S is the surface gradient operator and E_T is the coefficient of interfacial thermal elasticity, [cf. Eq. (1)]. The drops moving with different thermocapillary velocities can collide and flocculate or coalesce; this is the *thermal coagulation*.

B. Kinetics of Irreversible Coagulation

1. Basic Equations

The kinetic theory of the fast irreversible coagulation was first developed by Smoluchowski (173, 174) and later extended to the case of slow and reversible coagulation. In any case of coagulation the general set of kinetic equations reads (175):

$$\frac{dn_k}{dt} = \frac{1}{2}\sum_{i=1}^{k-1} a_f^{i,k-i} n_i n_{k-i} - n_k \sum_{i=1}^{\infty} a_f^{k,i} n_i + q_k \qquad (k = 1, 2, \ldots) \tag{96}$$

where t is time, n_1 denotes the number of single drops per unit volume, n_k is the number of floes of k drops (k = 2, 3,…,) per unit volume, and $a^{i,j}_f(i, j = 1, 2, 3,\ldots,)$ are rate constants of flocculation (see Fig. 19); q_k denotes a flux of

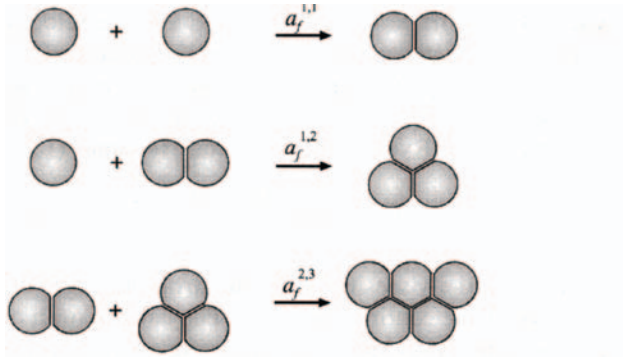

Figure 19 Examples for elementary acts of flocculation according to the Smoluchowski scheme; $a^{i,j}_f(i, j = 1, 2, 3,\ldots,)$ denote the respective rate constants of flocculation.

floes of size k which are products of other processes, different from the *flocculation* itself [say, the reverse process of floc disassembly, or the droplet coalescence, see Eqs (116) and (120)]. Analogously to flocculation, the *coalescence* in emulsions can be considered as a kind of irreversible coagulation (176—179).

In the special case of *irreversible* coagulation one has q_k=0. The first term on the right-hand side of Eq. (96) is the rate of formation of k floes by merging of two smaller floes, whereas the second term expresses the rate of disappearance of k flocs due to their incorporation into larger flocs. The total concentration of flocs (as kinetically independent units), n, and the total concentration of the constituent drops (including those in flocculated form), n_{tot}, are given by the expressions:

$$n = \sum_{k=1}^{\infty} n_k, \qquad n_{\text{tot}} = \sum_{k=1}^{\infty} k n_k \tag{97}$$

The rate constants in Eq. (96) can be expressed in the form:

$$a_f^{i,j} = 4\pi D_{i,j}^{(0)}(R_i + R_j)E_{i,j} \tag{98}$$

where $D^{(0)}{}_{i,j}$ is the relative diffusion coefficients for two flocs of radii R_i and R_j, and aggregation number i and j, respectively; and $E_{i,j}$ is the collision efficiency (180, 181). Below we give expressions for $D^{(0)}{}_{i,j}$ and $E_{i,j}$ applicable to the various types of coagulation.

The Einstein approach to the theory of diffusivity D gives the following expression:

$$D = kT/B, \qquad B \equiv F/V \tag{99}$$

where B is the friction coefficient, and V is the velocity acquired by a given particle under the action of an applied net force F. For a solid sphere of radius R_0 one has $B = 6\pi\eta R_0$. For a liquid drop, B is given by the equation of Rybczynski (182) and Hadamar (183):

$$B = 2\pi\eta R_0 \frac{3\eta_d + 2\eta}{\eta_d + \eta} \tag{100}$$

where η_d is the viscosity inside the drop, and η is the viscosity of the continuous phase. The combination of Eqs (99) and (100) yields the following expression for the relative diffusivity of two isolated Brownian droplets of radii R_i and R_j.

$$D^{(0)}_{i,j} = \frac{kT}{2\pi\eta}\frac{\eta_d + \eta}{3\eta_d + 2\eta}\left[\frac{1}{R_i} + \frac{1}{R_j}\right] \tag{101}$$
(perikinetic coagulation)

The limiting case $\eta_d \to 0$ corresponds to two bubbles, whereas in the other limit, $\eta_d \to \infty$, Eq. (101) describes two solid particles or two liquid drops of tangentially immobile surfaces.

When the relative motion of the drop is driven by a *body force* or by *thermocapillary migration* (rather than by self-diffusion), Eq. (101) is no longer valid. Instead, in Eq. (98) one has formally to substitute the following expression for $D^{(0)}{}_{i,j}$, see Rogers and Davis (184):

$$D^{(0)}_{i,j} = \frac{1}{4}(R_i + R_j)\,|\,\mathbf{v}_i - \mathbf{v}_j\,| \tag{102}$$
(orthokinetic coagulation)

Here, v_j denotes the velocity of a floc of aggregation number j. Physically, Eq. (102) accounts for the fact that the drops/flocs of different size move with different velocities under the action of the body force. In the case of gravity-driven flocculation v_j, is the velocity of a rising/sedimenting particle, which for a drop of tangentially immobile surface is given by the Stokes formula:

$$\mathrm{v}_j = \mathrm{v}_{\mathrm{bf}} \equiv 2g\,\Delta\rho R_j^2/(9\eta) \tag{103}$$
(sedimentation velocity)

see, e.g., Ref. 16; here, g is the acceleration due to gravity, and $\Delta\rho$ is the density difference between the two liquid phases.

In the case of *thermal coagulation*, the drop velocity v_j is given by the expression (185):

$$\mathbf{v}_j = \mathbf{v}_{\mathrm{tm}} \equiv \frac{2R_j E_T \lambda}{(3\eta_d + 2\eta)(\lambda_d + 2\lambda)}\nabla(\ln T) \tag{104}$$
(thermocapillary velocity)

where the thermal conductivity of the continuous and disperse phases are denoted by μ, and μ_d; the interfacial thermal elasticity E_T is defined by Eq. (95).

The *collision efficiency* $E_{i,j}$ in Eq. (98) accounts for the interactions (of both hydrodynamic and intermolecular origin) between two colliding drops. The inverse of E_T is called the *stability ratio* or the *Fuchs factor* (186) and can be expressed in the following general form (3, 180):

$$\Phi_{i,j} = \frac{1}{E_{i,j}} = 2\int_0^\infty \frac{\beta(s)}{(s+2)^2}\exp\left[\frac{W_{i,j}(s)}{kT}\right]\mathrm{d}s, \tag{105}$$

$$s \equiv \frac{2h}{R_i + R_j}$$

$$\beta \equiv \left[2\pi\eta a\frac{3\eta_d + 2\eta}{\eta_d + \eta}\right]^{-1} B(s) \tag{106}$$

As usual, h is the closest surface-to-surface distance between the two drops; a is defined by Eq. (46); $W_T(s)$ is the energy of *non hydrodynamic* interactions between the drops, see Eq. (67); $\beta(s)$ accounts for the *hydrodynamic* interactions; and $B(s)$ is the drop friction coefficient. For $s \to \infty$ one obtains $\beta \to 1$, since for large separations the drops obey the Rybczynski - Hadamar equation (100). In the opposite limit, $s \ll 1$, i.e., close approach of the two drops, $B(s) = F/V$ can be calculated from either Eq. (47), (49), (52), or (56), depending on the specific case. In particular, for $s \ll 1$ one has $\beta \propto s^{-1/2}$ for two spherical droplets of tangentially *mobile* surfaces, whereas $\beta \propto 1/s$ for two drops of tangentially *immobile* surfaces (or two solid particles). In the latter case the integral in Eq. (105) seems to be divergent. To overcome this problem it is usually accepted that for the smallest separations $W_{i,j}$ is dominated by the van der Waals attraction, i.e., $W_{i,j} \to -\infty$ for $s \to 0$, and consequently, the integrand in Eq. (105) tends to zero for $s \to 0$.

The Fuchs factor $\Phi_{i,j}$ is determined mainly by the values of the integrand in the vicinity of the electrostatic maximum (barrier) of $W_{i,j}$ (cf. Fig. 6a) since $W_{i,j}$ enters Eq. (105) as an exponent. By using the method of the saddle point, Derjaguin (3) estimated the integral in Eq. (105):

$$\Phi_{i,j} \equiv \frac{1}{E_{i,j}} \approx \left[\frac{8\pi kT}{-W''_{i,j}(s_m)}\right]^{1/2}\frac{\beta(s_m)}{(s_m+2)^2}\exp\left[\frac{W_{i,j}(s_m)}{kT}\right] \tag{107}$$

Here, S_m denotes the value of s corresponding to the maximum. One sees that the higher the barrier, $W_{i,j}(S_m)$, the

smaller the collision efficiency, $E_{i,j}$, and the slower the coagulation.

The infinite set of Smoluchowski equations [Eq. (96)] was solved by Bak and Heilmann (187) in the particular case when the floes cannot grow larger than a given size; an explicit analytical solution was obtained by these authors.

2. Special Results

For imaginary drops, which experience neither longrange surface forces ($W_{i,j} = 0$) nor hydrodynamic interactions ($\beta = 1$), Eq. (105) yields a collision efficiency $E_{i,j} = 1$, and Eq. (98) reduces to the Smoluchowski (173, 174) expression for the rate constant of *fast irreversible* coagulation. In this particular case, Eq. (96) represents an infinite set of nonlinear differential equations. If all flocculation rate constants are the same and equal to a_f, the problem has an exact analytical solution (173, 174):

$$n = \frac{n_0}{1 + a_f n_0 t/2}, \qquad n_k = n_0 \frac{(a_f n_0 t/2)^{k-1}}{(1 + a_f n_0 t/2)^{k+1}} \qquad (k = 1, 2 \ldots) \tag{108}$$

The total average concentration of the drops (in both singlet and flocculated form), n_{tot}, does not change and is equal to the initial number of drops, n_0. Unlike n_{tot}, the concentration of the floes, n, decreases with time, while their size increases. Differentiating Eq. (108) one obtains:

$$\frac{dn}{dt} = -\frac{a_f}{2} n^2, \qquad \frac{d\bar{V}}{dt} = \frac{a_f}{2}\phi_0, \qquad \bar{V} \equiv \frac{\phi_0}{n} \tag{109}$$

where $\bar{V}$ is the *average volume per floc*, and ϕ_0 is the initial volume fraction of the constituent drops. Combining Eqs (98) and (109) one obtains the following result for *perikinetic* (*Brownian*) coagulation:

$$\frac{\bar{V}}{V_0} = 1 + \frac{t}{t_{Br}}, \qquad t_{Br} = \frac{R_0^2}{3\phi_0 D_0 E_0} \tag{110}$$

where $V_0 = 4\pi R_0^3/3$ is the volume of a constituent drop of radius R_0, t_{Br} is the characteristic time of the coagulation process in this case, E_0 is an average collision efficiency, and D_0 is an average diffusion coefficient. Equation (110) shows that for fast irreversible coagulation, $\bar{V}$ increases linearly with time.

In contrast, $\bar{V}$ is not a linear function of time for *orthokinetic* coagulation, except in the limit of short times. When the flocculation is driven by a *body force*, i.e., in case of sedimentation or centrifugation, one obtains (181):

$$\frac{\bar{V}}{V_0} = \left(1 - \frac{t}{3t_{bf}}\right)^{-3}, \qquad t_{bf} = \frac{2R_0}{3\phi_0 v_{bf} E_0} \tag{111}$$

where t_{bf} is the characteristic time in this case, and v_{bf} is an average velocity of floc motion, which can be expressed by means of Eq. (103) if the body force is the gravitational one.

If the orthokinetic coagulation is driven by *thermocapillary migration*, the counterpart of Eq. (111) reads (181):

$$\frac{\bar{V}}{V} = \exp\left(\frac{t}{t_{tm}}\right) \qquad t_{tm} = \frac{2R_0}{3\phi_0 v_{tm} E_0} \tag{112}$$

where v_{tm} is an average velocity of thermocapillary migration, see Eq. (104), and t_{tm} is the respective characteristic time. Note that $D_0 \propto R_0^{-1}$, $v_{bf} \propto R_0^2$, and $v_{tm} \propto R_0$, cf. Eqs (99) and (104). From Eqs (110)-(112) it then follows that the three different characteristic times exhibit different dependencies on drop radius: $t_{Br} \propto R_0^3$, $t_{bf} \propto R_0^{-1}$, while t_{tm} is independent of R_0. Hence, the Brownian coagulation is faster for the smaller drops, and the body force-induced coagulation is more rapid for the larger drops, whereas the thermo-capillary-driven coagulation is not sensitive to the drop size.

Using the Stokes-Einstein expression for the diffusivity D_0 and Eq. (110) one obtains:

$$t_{Br} = \frac{2\pi\eta R_0^3}{\phi_0 kTE_0} \tag{113}$$

On the other hand, the combination of Eqs (103) and (111) yields:

$$t_{bf} = \frac{3\eta}{\phi_0 R_0 E_0 g \Delta\rho} \tag{114}$$

Let us consider the quantity:

$$\chi(R_0) \equiv \frac{t_{bf}}{t_{bf} + t_{Br}} = \frac{1}{1 + 3R_0^4/(5R_{cr}^4)}, \qquad R_{cr} = \left(\frac{9kT}{10\pi g \Delta\rho}\right)^{1/4} \tag{115}$$

For $R_0 < R_{cr}$, Eq. (115) yields $\chi(R_0) \approx 1$, i.e., $t_{br} \ll t_{bf}$, and the Brownian flocculation is much faster than the orthokinetic flocculation. In contrast, for $R_0 > R_{cr}$, Eq. (115) yields $\chi(R_0) \approx 0$, i.e., $t_{bf} \ll t_{Br}$, and the orthokinetic flocculation is much more rapid than the Brownian flocculation. At $R_0 = R_{cr}$, a sharp transition from Brownian to orthokinetic flocculation takes place; R_{cr} corresponds to the inflection point of the dependence $\chi = \chi(R_0)$. Since the orthokinetic

flocculation happens through a directional motion of the particles, then R_{cr} can be considered as a *threshold radius of the flocs* needed for the creaming (or sedimentation) to begin. With $\Delta\rho = 0.1$ g/cm^3 and $T = 298$ K from Eq. (115) one calculates $R_{cr} = 1.05$ μm. It turns out that the threshold size for creaming is around 1 μm. This conclusion is consistent with the experimental data in Fig. 3, which show that emulsions with $2R_0 = 5$ μm do cream, whereas those with $2R_0 = 0.35$ μm do not.

C. Kinetics of Reversible Flocculation

If the depth of the primary minimum (that on the left from the maximum in Fig. 6a) is not so great, i.e., the attractive force which keeps the drops together is weaker, then the floes formed are labile and can disassemble into smaller aggregates. This is the case of *reversible flocculation* (3). For example, a floc composed of i+j drops can be split into two flocs containing i and j drops. We denote the rate constant of this *reverse* process by $a^{i,j}{}_r$ (see Fig. 20a). In the present case both the straight process of flocculation (Fig. 19) and the reverse process (Fig. 20a) take simultaneously place. The kinetics of aggregation in this more general and complex case is described by the Smoluchowski set of equations, Eq. (96), where one is to substitute:

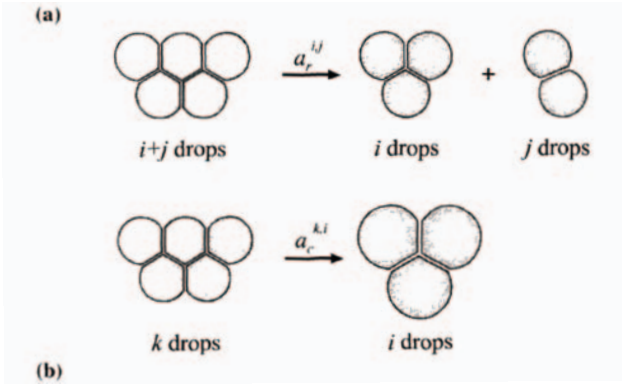

Figure 20 (a) elementary act of splitting of a floc, containing $i + j$ constitutive drops, into two smaller flocs containing, respectively, i and j constitutive drops; (b) coalescence transforms a floc composed of k drops into a floc containing i drops ($i < k$). The rate constants of the respective processes are $a^{i,j}{}_r$ and $a^{k,i}{}_c$ ($i, j, k = 1, 2, 3,\ldots$).

$$q_1 = \sum_{i=1}^{\infty} a_r^{1,i} n_{i+1}, \quad q_k = \sum_{i=1}^{\infty} a_r^{k,i} n_{i+k} - \frac{1}{2} n_k \sum_{i=1}^{k-1} a_r^{i,k-i} \quad (k = 2, 3, \ldots) \tag{116}$$

Here, q_k is the rate of formation of k flocs in the process of disassembly of larger flocs minus the rate of decay of the k flocs. As before, the total number of constituent drops, n_{tot}, does not change. However, the total number of the flocs, n, can either increase or decrease depending on whether the straight or the reverse process prevails. Summing up all equations in Eq. (96) and using Eq. (116) one derives the following equation for n:

$$\frac{dn}{dt} = \frac{1}{2} \sum_{i=1}^{\infty} \sum_{j=1}^{\infty} \left(a_r^{i,j} n_{i+j} - a_f^{i,j} n_i n_j \right) \tag{117}$$

A general expression for the rate constants of the reverse process was obtained by Martinov and Muller (188):

$$a_r^{i,j} = \frac{D_{i,j}^{(0)} E_{i,j}}{Z_{i,j}} \frac{1}{(R_i + R_j)^2} \tag{118}$$

Here, $Z_{i,j}$ is the so-called *irreversible factor*, which is defined as follows:

$$Z_{i,j} = \frac{1}{8} \int_{Wi,j<0} (s+2)^2 \exp\left[-\frac{W_{i,j}(s)}{kT} \right] ds \tag{119}$$

The integration in Eq. (119) is carried out over the region around the primary minimum, where $W_{i,j}$ takes negative values (cf. Fig. 6a). In other words, $Z_{i,j}$ is determined by the values of $W_{i,j}$ in the region of the primary *minimum*, whereas $E_{i,j}$ is determined by the values of $W_{i,j}$ in the region of the electrostatic *maximum*, cf. Eqs (107) and (119). When the minimum is deeper, $Z_{i,j}$ is larger and the rate constant in Eq. (118) is smaller. Moreover, Eqs (107) and (118) show that the increase in the height of the barrier also decreases the rate of the reverse process. The physical interpretation of this fact is the following: to detach a drop from a floc, the drop has to first emerge from the well and then to "jump" over the barrier (cf. Fig. 6a).

As an illustration, in Fig. 21 we show theoretical curves for the rate of flocculation calculated in Ref. 62. The curves are computed by solving numerically the set of Eqs (96), (116), and (117). To simplify the problem the following assumptions have been used (62): (1) the Smoluchowski assumption that all rate constants of the *straight* process are equal to a_f; (2) flocs containing more than M drops cannot

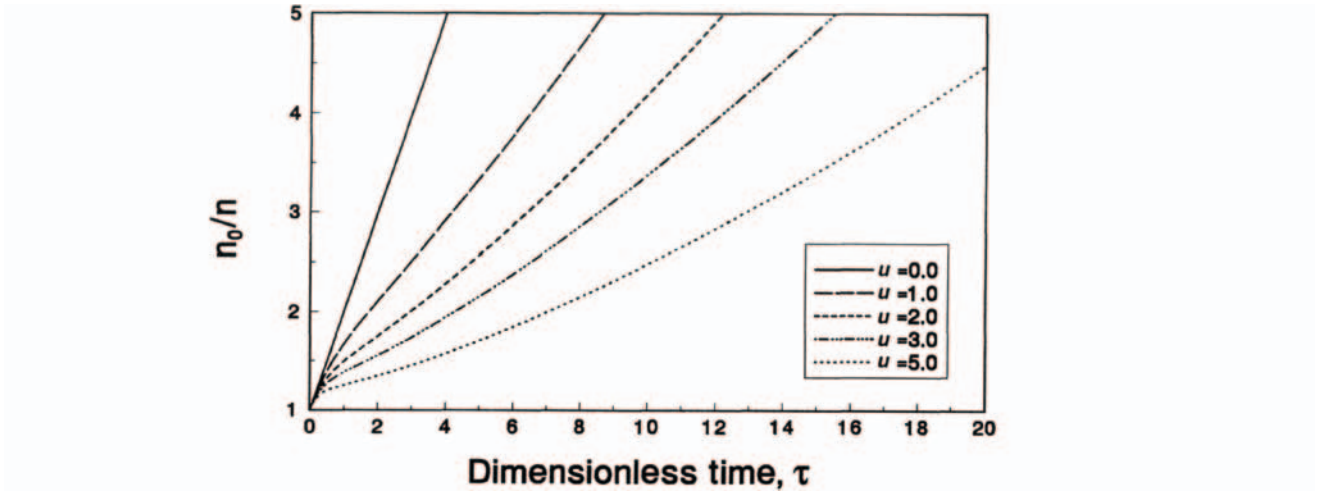

Figure 21 Plot of the inverse dimensionless concentration of flocs, n_0/n, vs. the dimensionless time, $\tau = a_f n_0 t/2$, for $M = 4$ and various values of the dimensionless ratio $u = 2a_r/(n_0 a_f)$; *ar* and *af* are the rate constants for the reverse and straight processes. Theoretical curves for reversible flocculation from Ref. 62.

decay; (3) all rate constants of the reverse process are equal to a_r; and (4) at the initial moment only single constituent drops of concentration n_0 are available. In Fig. 21 we present the calculated curves for n_0/n versus the dimensionless time, $\tau = a_f n_0 t/2$, for a fixed value $M = 4$ and various values of the ratio of the rate constants of the straight and the reverse process, $u = 2a_r/(n_0 a_f)$. Note that n is defined by Eq. (97). The increase in n_0/n with time means that the concentration n of the flocs decreases; i.e., the emulsion contains a smaller number of flocs, but their size is larger. Consequently, a larger n_0/n corresponds to a larger degree of flocculation. It is seen that for the short times of flocculation ($\tau \to 0$) all curves in Fig. 21 touch the Smoluchowski distribution (corresponding to $u = 0$), but for the longer times one observes a reduction in the degree of flocculation, which is smaller for the curves with larger values of u (larger rate constants of the reverse process). The "S-shaped" curves in Fig. 21 are typical for the case of *reversible* flocculation; curves of similar shape have been obtained experimentally (3, 168, 189).

D. Kinetics of Simultaneous Flocculation and Coalescence

In the case of *pure* flocculation considered above the total number of constituent drops, n_{tot}, does not change, see Eq. (97). In contrast, if coalescence is present, in addition to the flocculation, then n_{tot} decreases with time (6). Hartland and Gakis (190) and Hartland and Vohra (191) developed a model of coalescence, which relates the lifetime of single films to the rate of phase separation in emulsions of comparatively large drops (> 1 mm) in the *absence* of surfactant. The effect of surfactant (emulsifier) was taken into account by Lobo et al. (192), who quantified the process of coalescence within an already creamed or settled emulsion containing drops of size less than 100 μm. Danov et al. (175) generalized the Smoluchowski scheme of flocculation to account for the fact that the droplets within the flocs can coalesce to give larger droplets, as illustrated in Fig. 20b. In this case, on the right-hand side of Eq. (96) one has to substitute (175):

$$q_1 = \sum_{i=2}^{\infty} a_c^{i,1} n_i ,$$

$$q_k = \sum_{i=k+1}^{\infty} a_c^{i,k} n_i - n_k \sum_{i=1}^{k-1} a_c^{k,i} \qquad (k = 2, 3, \ldots) \tag{120}$$

where $a^{k,i}{}_c$ is the rate constant of transformation (by coalescence) of a floc containing k droplets into a floc containing i droplets (see Fig. 20b). The resulting floc is further involved in the flocculation scheme, which thus describes the interdependence of flocculation and coalescence. In this scheme the total coalescence rate, $a^i{}_{c,tot}$, and the total number of droplets, n_{tot}, are related as follows (175):

$$\frac{dn_{tot}}{dt} = -\sum_{i=2}^{\infty} a_{c,tot}^{i} n_i ,$$

$$a_{c,tot}^{i} = \sum_{k=1}^{i-1} (i-k) a_c^{i,k} \qquad (i = 2, 3, \ldots) \tag{121}$$

To determine the rate constants of coalescence, $a^{k,i}_c$, Danov et al. (147) examined the effects of the droplet interactions and the Brownian motion on the coalescence rate in dilute emulsions of micrometer- and submicrometer-sized droplets. The processes of film formation, thinning, and rupture were included as consecutive stages in the scheme of coalescence. Expressions for the interaction energy due to various DLVO and nonDLVO surface forces between two deformed droplets were obtained (143).

Average models for the total number of droplets have also been proposed (193, 194). The average model of van den Tempel (193) assumes a linear structure for the flocs. The coalescence rate is supposed to be proportional to the number of contacts within a floc. To simplify the problem van den Tempel used several assumptions, one of them being that the concentration of the single droplets, n_1, obeys the Smoluchowski distribution, Eq. (108), for k=1. The model of Borwankar et al. (194) employs some assumptions, which make it more applicable to cases in which the flocculation (rather than the coalescence) is slow and is the rate-determining stage. This is illustrated by the curves shown in Fig. 22, which are calculated for the same rate of *coalescence*, but for two different rates of *flocculation*. For relatively high rates of flocculation (Fig. 22a) the predictions of the three theories differ, but the model of Borwankar et al. (194) gives values closer to that of the more detailed model by Danov et al. (175). For very low values of the flocculation rate constant, a_f, for which the coalescence is not the rate-determining stage, all three theoretical models (175, 193, 194) give results for n_{tot}/n_0 versus time, which almost coincide numerically (Fig. 22b).

Finally, it is worthwhile noting that the simultaneous flocculation and coalescence in emulsions could be also accompanied with adsorption of amphiphilic molecules on the drop surfaces (195); this possibility should be kept in mind when interpreting experimental data.

VII. SUMMARY

Surfactants play a crucial role in emulsification and emulsion stability. A first step in any quantitative study on emulsions should be to determine the equilibrium and dynamic properties of the oil-water interface, such as interfacial tension, Gibbs elasticity, surfactant adsorption, counterion binding, surface electric potential, adsorption relaxation time, etc. Useful theoretical concepts and expressions, which are applicable to ionic, nonionic, and micellar surfactant solutions, are summarized in Sec. II.

The emulsion drops in floes and creams are separated with thin liquid films, whose rupture leads to coalescence and phase separation. At equilibrium the area of the films and their contact angle are determined by the surface forces (disjoining pressure) acting across the films (Sec. III.A.1). Several ways of breakage of these emulsion films have been established: capillary-wave mechanism, pore-nucleation mechanism, solute-transport mechanism, barrier mechanism, etc. (Sec. III.A.2).

Experimental and theoretical results show evidence that the capillary-wave mechanism is the most frequent reason for the coalescence of both deformed and spherical emulsion drops. For a certain critical thickness (width), h_c, of the film (gap) between two emulsion drops the amplitude of the thermally excited fluctuation capillary waves begins to grow, promoted by the surface forces, and causes film rupture. The capillary waves can bring about coalescence of two spherical emulsion drops, when the distance between them becomes smaller than a certain critical value, which is estimated to be about 10—50 nm (see Sec. III.C).

The interactions of two emulsion drops, and their theoretical description, become more complicated if the drops are moving against each other, instead of being quiescent. In such a case, which happens most frequently in practice, the hydrodynamic interactions come into play (Sec. IV). The velocity of approach of two drops and the critical distance (thickness) of drop coalescence are influenced by the drop size, disjoining pressure, bulk and surface diffusivity of surfactant, Gibbs elasticity, surface viscosity, etc. If attractive (negative) disjoining pressure prevails, then "pimples" appear on the opposite drop surfaces in the zone of contact; thus, the drop coalescence can be produced by the growth and merging of these "pimples" (Sec. IV.A.3). Alternatively, drop coalescence can be produced by the growth of fluctuation capillary waves; the theory of the respective critical thickness is found to agree excellently with available experimental data (Sec. IV.B.3).

The finding that the hydrodynamic velocity of mutual approach of two emulsion drops is much higher when the surfactant is dissolved in the drop phase (rather than in the continuous phase) provides a natural explanation of the Bancroft rule in emulsification (Sec. V). A generalized version of the Bancroft rule is proposed, Eqs (89) and (91), which takes into account the role of various thermodynamic and hydrodynamic factors. For example, the existence of a considerable repulsive (positive) disjoining pressure may lead to exclusions from the conventional Bancroft rule, which are accounted for in its generalized version.

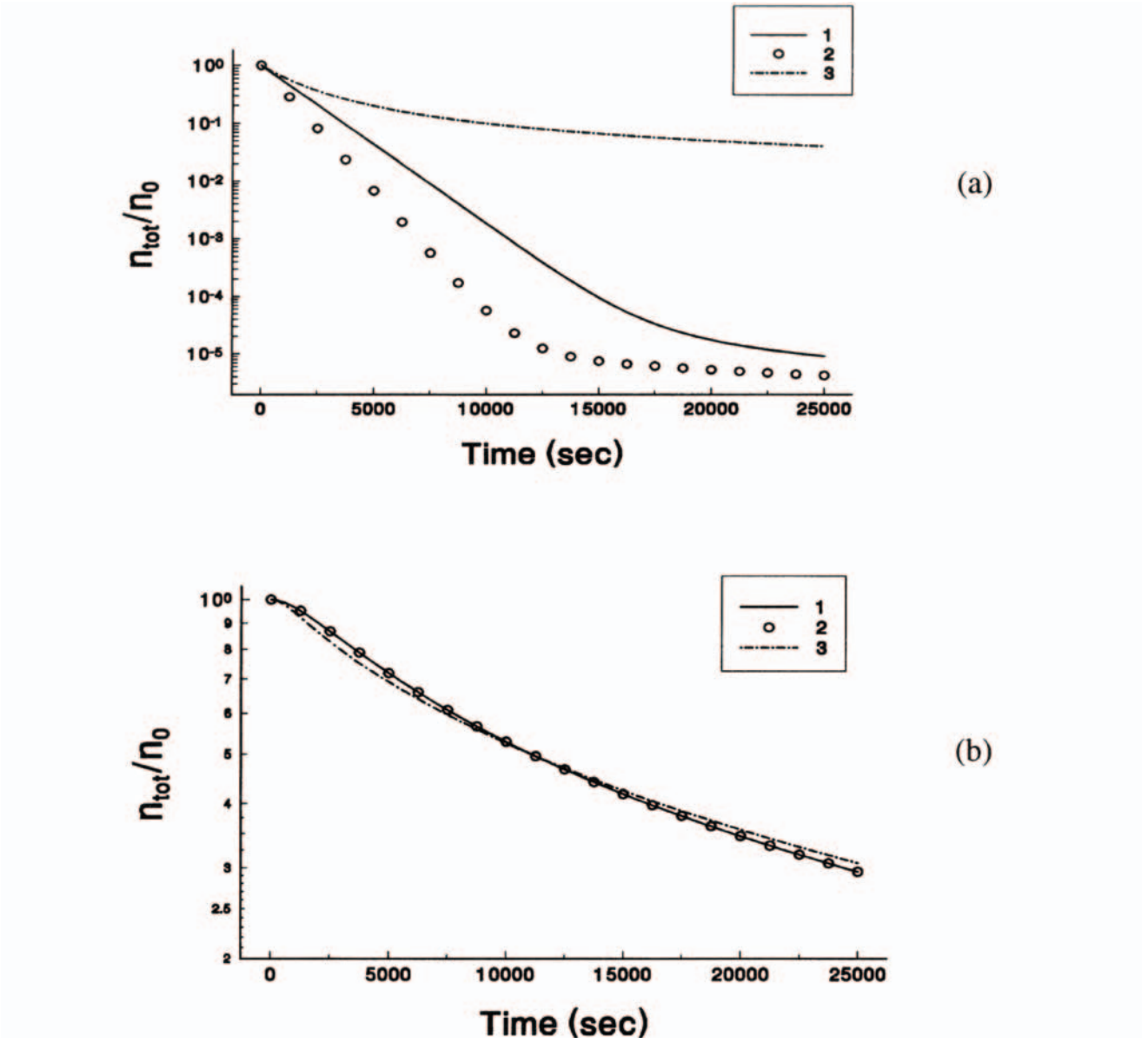

Figure 22 The total number of constituent drops in a flocculating emulsion, n_{tot}, decreases with time, t, because of a parallel process of coalescence. The curves are calcualted for the following parameter values: initial number of constituent drops $n_0 = 10^{12}cm^{-3}$; coalescence rate constant $k^{2,1}{}_c = 10^{-3}$ s^{-1}. Curve 1 is a numberical solution to Eq. (121); Curves 2 and 3 are the results predicted by the models of Borwankar *et al*. (194) and van den Tempel (193), respectively. The values of the flocculation rate constant are: (a) $a_f = 10^{-11}$ cm^3/s; (b) $a_f = 10^{-16}$ cm^3/s.

Knowledge concerning the individual acts of drop-drop collision is a prerequisite for development of a kinetic theory of such collective phenomena as flocculation/coalescence and phase separation. The cases of fast and slow, perikinetic and orthokinetic, and irreversible and reversible flocculation are considered in Sec. VI. Special attention is paid to the case of parallel flocculation and coalescence. Much work remains to be done in order to build up united theory including both individual drop interactions and collective phenomena in emulsions.

ACKNOWLEDGMENTS

Financial Support from the Inco-Copernicus Project No. 1C 15 CT98 0911 of the European Commission is gratefully acknowledged. The authors are indebted to Ms Mariana Paraskova and Mr Vesselin Kolev for their help in the preparation of the figures.

REFERENCES

1. IB Ivanov, PA Kralchevsky. Colloids Surfaces A 128: 155—175, 1997.
2. IB Ivanov, KD Danov, PA Kralchevsky. Colloids Surfaces A 152: 161—182, 1999.
3. BV Derjaguin. Theory of Stability of Colloids and Thin Films. New York: Plenum Press - Consultants Bureau, 1989.
4. JN Israelachvili. Intermolecular & Surface Forces. London: Academic Press, 1992.
5. VM Mikova. Investigation of Emulsions Stabilized by ß-Lactoglobulin. MSc thesis, University of Sofia, 1999.
6. JT Davies, EK Rideal. Interfacial Phenomena. London: Academic Press, 1963.
7. PC Hiemenz, R Rajagopalan. Principles of Colloid and Surface Chemistry. New York: Marcel Dekker, 1997.
8. I Langmuir. J Am Chem Soc 15: 75—84, 1918.
9. TL Hill. An Introduction to Statistical Thermodynamics. Reading, MA: Addison-Wesley, 1962.
10. M Volmer. Z Phys Chem 115: 253—259, 1925.
11. A Frumkin. Z Phys Chem 116: 466—475, 1925.
12. LD Landau, EM Lifshitz. Statistical Physics. Part 1. Oxford: Pergamon Press, 1980.
13. TD Gurkov, PA Kralchevsky, K Nagayama. Colloid Polym Sci 274: 227—238, 1996.
14. EH Lucassen-Reynders. J Phys Chem 70: 1777—1785, 1966.
15. RP Borwankar, DT Wasan. Chem Eng Sci 43: 1323—1337, 1988.
16. ED Shchukin, AV Pertsov, EA Amelina. Colloid Chemistry. Moscow: Moscow University Press, 1982 (in Russian).
17. PA Kralchevsky, KD Danov, G Broze, A Mehreteab. Langmuir 15: 2351—2365, 1999.
18. JW Gibbs. The Scientific Papers of J. W. Gibbs. Vol 1. New York: Dover, 1961.
19. EH Lucassen-Reynders. In: P Becher, ed. Encyclopedia of Emulsion Technology. Vol 4. New York: Marcel Dekker, 1996, p 63.
20. Y Tian, RG Holt, R Apfel. J Colloid Interface Sci, 187: 1—10, 1997.
21. A Ozawa, A Minamisawa, K Sakai, K Takagi. Jpn J Appl Phys 33: L-1468, 1994.
22. K Sutherland. Austr J Sci Res Ser A 5: 683—689, 1952.
23. SS Dukhin, G Kretzschmar, R Miller. Dynamics of Adsorption at Liquid Interfaces. Amsterdam: Elsevier, 1995.
24. KD Danov, PA Kralchevsky, IB Ivanov. In: G Broze, ed. Handbook of Detergents. New York: Marcel Dekker, 1999, p 303.
25. JTG Overbeek. In: HR Kruyt, ed. Colloid Science. Vol 1. Amsterdam: Elsevier, 1953; J Colloid Sci 8: 420, 1953.
26. G Gouy. J. Phys Radium 9: 457—466, 1910.
27. DL Chapman. Phil Mag 25: 475—485, 1913.
28. O Stern. Z. Elektrochem 30: 508—512, 1924.
29. S Hachisu. J Colloid Interface Sci 33: 445—455, 1970.
30. DG Hall. In: DM Bloor, E Wyn-Jones, eds. The Structure, Dynamics and Equilibrium Properties of Colloidal Systems. Dordrecht: Kluwer, 1990, p 857.
31. DG Hall. Colloids Surfaces A 90: 285—293, 1994.
32. G Bakker. Handbuch der Experimentalphysik. Band 6. Leipzig: Akademische Verlagsgesellschaft, 1928.
33. S Ono, S Kondo. In: S Flügge, ed. Handbuch der Physik. Vol 10. Berlin: Springer, 1960, p 134.
34. JS Rowlinson, B Widom. Molecular Theory of Capillarity. Oxford: Clarendon Press, 1982.
35. KD Danov, PM Vlahovska, PA Kralchevsky, G Broze, A Mehreteab. Colloids Surfaces A 156: 389—411, 1999.
36. KD Danov, VL Kolev, PA Kralchevsky, G Broze, A Mehreteab. Langmuir 16: 2942—2956, 2000.
37. VV Kalinin, CJ Radke. Colloids Surfaces A 114: 337—350, 1996.
38. K Tajima, M Muramatsu, T Sasaki. Bull Chem Soc Jpn 43: 1991—1998, 1970.
39. K Tajima. Bull Chem Soc Jpn 43: 3063—3067, 1970.
40. E Janke, F Emde, F Lösch. Tables of Higher Functions. New York: McGraw-Hill, 1960.
41. M Abramowitz, IA Stegun. Handbook of Mathematical Functions. New York: Dover, 1965.
42. GA Korn, TM Korn. Mathematical Handbook. New York: McGraw-Hill, 1968.
43. G Loglio, E Rillaerts, P Joos. Colloid Polym Sci 259: 1221—1230, 1981.
44. R Miller. Colloid Polym Sci 259: 375-381, 1981.
45. YM Rakita, VB Fainerman, VM Zadara. Zh Fiz Khim 60: 376—388, 1986.
46. PA Kralchevsky, YS Radkov, ND Denkov. J Colloid Interface Sci 161: 361-=365, 1993.
47. KD Danov, PM Vlahovska, TS Horozov, CD Dushkin, PA Kralchevsky, A Mehreteab, G Broze. J Colloid Interface Sci 183: 223—235, 1996.
48. RS Hansen. J Chem Phys 64: 637, 1960.
49. R van den Bogaert, P Joos. J Phys Chem 83: 2244—2251, 1979.
50. E Rillaerts, P Joos. J Chem Phys 96: 3471—3477, 1982.
51. R Miller, G Kretzchmar. Adv Colloid Interface Sci 37: 97—136, 1991.
52. VB Fainerman, AV Makievski, R Miller. Colloids Surfaces A 87: 61—75, 1994.
53. LK Filippov. J Colloid Interface Sci 164: 471—482, 1994.
54. A Bonfillon, F Sicoli, D Langevin J Colloid Interface Sci 168: 497—504, 1994.
55. C MacLeod, CJ Radke. Langmuir 10: 2965—2975, 1994.
56. AW Cross, GG Jayson. J Colloid Interface Sci 162: 45—

53, 1994.
57. SB Johnson, CJ Drummond, PJ Scales, S Nishimura. Langmuir 11: 2367—2378, 1995.
58. RG Alargova, KD Danov, JT Petkov, PA Kralchevsky, G Broze, A Mehreteab. Langmuir 13: 5544—5551, 1997.
59. OD Velev, TD Gurkov, RP Borwankar. J Colloid Interface Sci 159: 497—501, 1993.
60. KD Danov, TD Gurkov, TD Dimitrova, D Smith. J Colloid Interface Sci 188: 313—324, 1997.
61. OD Velev, TD Gurkov, IB Ivanov, RP Borwankar. Phys Rev Lett 7—75: 264—267, 1995.
62. PA Kralchevsky, KD Danov, ND Denkov. In: KS Birdi, ed. Handbook of Surface and Colloid Chemistry. Boca Raton, L: CRC Press, 1997, p 333.
63. MJ Rosen. Surfactants and Interfacial Phenomena. New York: John Wiley, 1989.
64. J Clint. Surfactant Aggregation. London: Chapman & Hall, 1992.
65. EAG Aniansson, SN Wall. J Phys Chem 78: 1024—1030, 1974.
66. EAG Aniansson, SN Wall. J Phys Chem 79: 857—864, 1975.
67. EAG Aniansson, SN Wall. In: E Wyn-Jones, ed: Chemical and Biological Applications of Relaxation Spectrometry. Dordrecht: Reidel, 1975, p 223.
68. EAG Aniansson, SN Wall, M Almgren, H Hoffmann, I Kielmann, W Ulbricht, R Zana, J Lang, C Tondre. J Phys Chem 80: 905—922, 1976.
69. CD Dushkin, IB Ivanov. Colloids Surfaces 60: 213—233, 1991.
70. CD Dushkin, IB Ivanov, PA Kralchevsky. Colloids Surfaces 60: 235—261, 1991.
71. BA Noskov. Kolloidn Zh 52: 509—517, 1990.
72. BA Noskov. Kolloidn Zh 52: 796—805, 1990.
73. GC Kresheck, E Hamori, G Davenport, HA Scheraga. J Am Chem Soc 88: 264—279, 1966.
74. PA Kralchevsky, IB Ivanov. Chem Phys Lett 121: 111—116, 1985.
75. IB Ivanov, PA Kralchevsky. In: IB Ivanov, ed. Thin Liquid Films. New York: Marcel Dekker, 1988, p49.
76. IB Ivanov, BV Toshev. Colloid Polym Sci 253: 593—599, 1975.
77. JA. de Feijter, A Vrij. J Colloid Interface Sci 70: 456—467, 1979.
78. PA Kralchevsky, ND Denkov. Chem Phys Lett 240: 385—392, 1995.
79. AD Nikolov, DT Wasan, PA Kralchevsky, IB Ivanov. In: N Ise, I Sogami, eds. Ordering and Organisation in Ionic Solutions. Singapore: World Scientific, 1988, p 302.
80. AD Nikolov, DT Wasan. J Colloid Interface Sci 133: 1—12, 1989.
81. AD Nikolov, PA Kralchevsky, IB Ivanov, DT Wasan. J Colloid Interface Sci 133: 13—22, 1989.
82. PA Kralchevsky, AD Nikolov, DT Wasan, IB Ivanov. Langmuir 6: 1180—1189, 1990.
83. AD Nikolov, DT Wasan, ND Denkov, PA Kralchevsky, IB Ivanov. Prog Colloid Polym Sci 82: 87—98, 1990.
84. DT Wasan, AD Nikolov, PA Kralchevsky, IB Ivanov. Colloids Surfaces 67: 139—145, 1992.
85. V Bergeron, CJ Radke. Langmuir 8: 3020—3026, 1992.
86. JL Parker, P Richetti, P Kékicheff, S Sarman. Phys Rev Lett 68: 1955—1958, 1992.
87. ML Pollard, CJ Radke. J Chem Phys 101: 6979—6991, 1994.
88. XL Chu, AD Nikolov, DT Wasan. Langmuir 10: 4403—4408, 1994.
89. XL Chu, AD Nikolov, DT Wasan. J Chem Phys 103: 6653—6661, 1995.
90. ES Basheva, KD Danov, PA Kralchevsky. Langmuir 13: 4342—4348, 1997.
91. KG Marinova, TD Gurkov, TD Dimitrova, RG Alargova, D Smith. Langmuir 14: 2011—2019, 1998.
92. AJ de Vries. Rec Trav Chim Pays-Bas 77: 44—53, 1958.
93. A Scheludko. Proc K Akad Wetensch B 65: 87—91, 1962.
94. A Vrij. Disc Faraday Soc 42: 23—31, 1966.
95. IB Ivanov, B Radoev, E Manev, A Scheludko. Trans Faraday Soc 66: 1262—1273, 1970.
96. IB Ivanov, DS Dimitrov. Colloid Polym Sci 252: 982—990, 1974.
97. IB Ivanov. Pure Appl Chem 52: 1241—1262, 1980.
98. PA Kralchevsky, KD Danov, IB Ivanov. In: RK Prud'homme, SA Khan, eds. Foams. New York: Marcel Dekker, 1995, p 1.
99. BV Derjaguin, YV Gutop. Kolloidn Zh 24: 431—438, 1962.
100. BV Derjaguin, AV Prokhorov. J Colloid Interface Sci 81: 108—115, 1981.
101. AV Prokhorov, BV Derjaguin. J Colloid Interface Sci 125: 111—123, 1988.
102. D Kashchiev, D Exerowa. J Colloid Interface Sci 77: 501—511, 1980.
103. D Kashchiev, D Exerowa. Biochim Biophys Acta 732: 133—142, 1983.
104. D Kashchiev. Colloid Polym Sci 265: 436—441, 1987.
105. YA: Chizmadzhev, VF Pastushenko. In: IB Ivanov, ed. Thin Liquid Films. New York: Marcel Dekker, 1988, p 1059.
106. LV Chernomordik, MM Kozlov, GB Melikyan, IG Abidor, VS Markin, YA Chizmadzhev. Biochim Biophys Acta 812: 643—655, 1985.
107. LV Chernomordik, GB Melikyan, YA Chizmadzhev. Biochim Biophys Acta 906: 309—352, 1987.
108. A Kabalnov, H Wennerstrom. Langmuir 12: 276—292, 1996.
109. IB Ivanov, SK Chakarova, BI Dimitrova. Colloids Surfaces 22: 311—316, 1987.
110. BI Dimitrova, IB Ivanov, E Nakache. J Dispers Sci Technol 9: 321—341, 1988.
111. KD, Danov, IB Ivanov, Z Zapryanov, E Nakache, S Raharimalala. In: MG Velarde, ed. Proceedings of the Conference of Synergetics, Order and Chaos. Singapore: World Scientific, 1988, p 178.
112. CV Sterling, LE Scriven. AIChE J 5: 514—520, 1959.
113. SP Lin, HJ Brenner. J Colloid Interface Sci 85: 59—74, 1982.

114. TD Gurkov, KD Danov, N Alleborn, H Raszillier, F Durst. J Colloid Interface Sci 198: 224—240, 1998.
115. J Lucassen, M van den Tempel, A Vrij, FT Hesselink. Proc Konkl Ned Akad Wet B 73: 109—113, 1970.
116. AK Malhotra, DT Wasan. Chem Eng Commun 48: 35—41, 1986.
117. C Maldarelli, RK Jain. In: IB Ivanov, ed. Thin Liquid Films: Fundamental and Applications. New York: Marcel Dekker, 1988, p 497.
118. BU Felderhof. J Chem Phys 49: 44—52, 1968.
119. S Sche, HM Fijnaut. Surface Sci 76: 186—198, 1978.
120. ED Manev, SV Sazdanova, DT Wasan. J Colloid Interface Sci 97: 591—604, 1984.
121. IB Ivanov, DS Dimitrov. In: IB Ivanov, ed. Thin Liquid Films. New York: Marcel Dekker, 1988, p. 379.
122. P Taylor. Proc Roy Soc (London) A108: 11—14, 1924.
123. E Rushton, GA Davies. Appl Sci Res 28: 37—42, 1973.
124. S Haber, G Hetsroni, A Solan. Int J Multiphase Flow 1: 57—66, 1973.
125. LD Reed, FA Morrison. Int J Multiphase Flow 1: 573—584, 1974.
126. G Hetsroni, S Haber. Int J Multiphase Flow 4: 1, 1978.
127. FA Morrison, LD Reed. Int J Multiphase Flow 4: 433—434, 1978.
128. VN Beshkov, BP Radoev, IB Ivanov. Int J Multiphase Flow 4: 563—570, 1978.
129. DJ Jeffrey, Y Onishi. J Fluid Mech 139: 261—276, 1984.
130. YO Fuentes, S Kim, DJ Jeffrey. Phys Fluids 31: 2445—2455, 1988.
131. RH Davis, JA Schonberg, JM Rallison. Phys Fluids Al: 77—81, 1989.
132. X Zhang, RH Davis. J Fluid Mech 230: 479—191, 1991.
133. TT Traykov, IB Ivanov. Int J Multiphase Flow 3: 471—483, 1977.
134. TT Traykov, ED Manev, IB Ivanov. Int J Multiphase Flow 3: 485—494, 1977.
135. IB Ivanov, BP Radoev, T Traykov, D Dimitrov, E Manev, C Vassilieff. In: E Wolfram, ed. Proceedings of the International Conference on Colloid and Surface Science. Vol 1. Budapest: Akademia Kiado, 1975, p 583.
136. KD Danov, IB Ivanov. Critical film thickness and coalescence in emulsions. Proceedings of the Second World Congress on Emulsions, Paris, 1997, Paper No. 2-3-154.
137. KD Danov, DS Valkovska, IB Ivanov. J Colloid Interface Sci 211: 291—303, 1999.
138. DS Valkovska, KD Danov, IB Ivanov. Colloids Surfaces A 156: 547—566, 1999.
139. SG Yanitsios, RH Davis. J Colloid Interface Sci 144: 412—432, 1991.
140. V Cristini, J Blawzdziewicz, M Loewenberg. J Fluid Mech 366: 259—273, 1998.
141. DS Valkovska, KD Danov, IB Ivanov. Colloids Surfaces A 175: 179—192, 2000.
142. O Reynolds. Phil Trans Roy Soc (London) A177: 157—234, 1886.
143. KD Danov, DN Petsev, ND Denkov, R Borwankar. J Chem Phys 99: 7179—7189, 1993.
144. ND Denkov, PA Kralchevsky, IB Ivanov, CS Vassilieff. J Colloid Interface Sci 143: 157—173, 1991.
145. ND Denkov, DN Petsev, KD Danov. Phys Rev Lett 71: 3226—3229, 1993.
146. DN Petsev, ND Denkov, PA Kralchevsky. J Colloid Interface Sci 176: 201—213 1995.
147. KD Danov, ND Denkov, DN Petsev, IB Ivanov, R Borwankar. Langmuir 9: 1731—1740, 1993.
148. A Scheludko, D Exerowa. Kolloid-Z 165: 148—157, 1959.
149. A Scheludko. Adv Colloid Interface Sci 1: 391—440, 1967.
150. OD Velev, AD Nikolov, ND Denkov, G Doxastakis, V Kiosseoglu, G Stalidis. Food Hydrocolloids 7: 55—71, 1993.
151. OD Velev, TD Gurkov, SK Chakarova, BI Dimitrova, IB Ivanov, RP Borwankar. Colloids Surfaces A 83: 43—55, 1994.
152. OD Velev, GN Constantinides, DG Avraam, AC Payatakes, RP Borwankar. J Colloid Interface Sci 175: 68—76, 1995.
153. KG Marinova, TD Gurkov, OD Velev, IB Ivanov, B Campbell RP Borwankar. Colloids Surfaces A 123/124: 155—167, 1997.
154. KP Velikov, OD Velev, KG Marinova, GN Constantinides. J Chem Soc Faraday Trans 93: 2069—2075, 1997.
155. OD Velev, KD Danov, IB Ivanov. J Dispers Sci Technol 18: 625—645, 1997.
156. KG Marinova, TD Gurkov, TD Dimitrova, RG Alargova, D Smith. Progr Colloid Polym Sci 110: 245—250, 1998.
157. OD Velev, BE Campbell, RP Borwankar. Langmuir 14: 4122—4130, 1998.
158. TD Gurkov, KG Marinova, A Zdravkov, C Oleksiak, B Campbell. Progr Colloid Polym Sci 110: 263—268, 1998.
159. BP Radoev, DS Dimitrov, IB Ivanov. Colloid Polym Sci 252: 50—55, 1974.
160. WB Russel, DA Saville, WR Schowalter. Colloidal Dispersions. Cambridge, England: Cambridge University Press, 1989, p 155.
161. WD Bancroft. J Phys Chem 17: 514—522, 1913.
162. BP Binks. Langmuir 9: 25—28, 1993.
163. KD Danov, OD Velev, IB Ivanov, RP Borwankar. Bancroft rule and hydrodynamic stability of thin films and emulsions. Proceedings of First World Congress on Emulsions, Paris, 1993.
164. H Kunieda, DF Evans, C Solans, M Yoshida. Colloids Surfaces A 47: 35—46, 1990.
165. MJ Schick. Nonionic Surfactants: Physical Chemistry. New York: Marcel Dekker 1986.
166. K Shinoda, S Friberg. Emulsions and Solubilization New York: John Wiley, 1986.
167. EE Isaacs, H Huang, AJ Babchin. Colloids Surfaces 46: 177—192, 1990; Colloids Surfaces A 123/124: 195—203, 1997.
168. O Holt, O Seather, J Sjöblom, SS Dukhin, NA Mishchuk. Colloids Surfaces A 123/124: 195—207, 1997.
169. K Demetreades, DJ McClements. Colloids Surfaces A 150: 45—54, 1999.
170. F Feuillebois. J Colloids Interface Sci 131: 267—275, 1989.

171. RM Merritt, RS Subramanian. J Colloid Interface Sci 131: 514—521, 1989.
172. KD Barton, RS Subramanian. J Colloid Interface Sci 133: 214—221, 1989.
173. M von Smoluchowski. Phys Z 17: 557—569, 1916.
174. M von Smoluchowski. Z Phys Chem 92: 129—143, 1917.
175. KD Danov, IB Ivanov, TD Gurkov, RP Borwankar. J Colloid Interface Sci 167: 8—17, 1994.
176. JL Klemaszewski, KP Das, JE Kinsella. J Food Sci 57: 366—371, 1992.
177. PT Jaeger, JJM Janssen, F Groneweg, WGM Agterof. Colloids Surfaces A, 85: 255—264, 1994.
178. E Dickinson, A Williams. Colloids Surfaces A 88: 317—326, 1994.
179. AJF Sing, A Graciaa, JL Salager. Colloids Surfaces A, 152: 31—39, 1999.
180. X Zhang, RH Davis. J Fluid Mech 230: 479—491, 1991.
181. H Wang, RH Davis. J Colloid Interface Sci 159: 108—118, 1993.
182. W Rybczynski. Bull Int Acad Sci (Cracovie) A, 40—49, 1911.
183. JS Hadamar. Comp Rend Acad Sci (Paris) 152: 1735—1740, 1911.
184. JR Rogers, RH Davis. Metal Trans A21: 59—68, 1990.
185. NO Young, JS Goldstein, MJ Block. J Fluid Mech 6: 350—365, 1959.
186. NA Fuchs. Z Phys 89: 736—742, 1934.
187. TA Bak, O Heilmann. J Phys A: Math Gen 24: 4889—4893, 1991.
188. GA Martinov, VM Muller. In: BV Derjaguin, ed. Research in Surface Forces. Vol 4. New York: Plenum Press - Consultants Bureau, 1975, p 3.
189. IM Elminyawi, S Gangopadhyay, CM Sorensen. J Colloid Interface Sci 144: 315—323, 1991.
190. S Hartland, N Gakis. Proc Roy Soc (London) A369: 137—148, 1979.
191. S Hartland, DK Vohra. J Colloid Interface Sci 77: 295—308, 1980.
192. LA Lobo, IB Ivanov, DT Wasan. AIChE J 39: 322—334, 1993.
193. M van den Tempel. Recueil 72: 419—461, 1953.
194. RP Borwankar, LA Lobo, DT Wasan. Colloids Surfaces 69: 135—144, 1992.
195. R Hogg. Colloids Surfaces A 146: 253—270, 1999.